Dye Sensitized Blue to UV-B Upconversion for Potential Light Therapy Applications

Master Thesis

Written by

Georgia Samara

Supervisors

Prof. dr. Andries Meijerink

dr. Dechao Yu

Universiteit Utrecht

Debye Institute for Nanomaterials Science

Condensed Matter & Interfaces

September 2019

Abbreviations

Room Temperature (RT)

Nitrogen Atmosphere (N_2)

Cyclohexane (CH)

Upconversion (UC)

Nanoparticles (NPs)

Perylene Propionic Acid (PPA_2)

Commercial Coumarin (CC)

Dye: NPs (Antenna: NPs)

Dye Molecules=Antenna Molecules

Upconversion Nanoparticles (UCNPS)

Förster Resonant Energy Transfer (FRET)

Narrow Band (NB)

Ultraviolet B (UVB)

Table of Contents

Abstract

UV-B light (311-313 nm) has been proven to treat skin disorders such as psoriasis and vitiligo[1][2][3]. Lanthanide ion doped phosphors are among the best for UC [4]and have been well studied for the IR-to-NIR[5] and NIR-to-Visible/UV processes[6][7]. Blue(~450nm) to UVB (~313nm) UC is a promising phototherapy method combining safer blue irradiation and topical UV-B light treatment which is beneficial for the patients. In this study, successful blue-to-UVB UC (~450nm to ~313nm) was realized in Ho^{3+}/Gd^{3+} co-doped $NaYF_4$ NPs; where the concentrations of Ho^{3+} and Gd^{3+} dopants were optimized to 1% and 25% respectively, with respect to the Y^{3+} lattice site. Due to the weak absorption of intra-4f transitions of Ho^{3+}, organic Dye molecules (super-broad blue absorption), are utilized as Förster Resonance Energy Transfer (FRET) sensitization antennas on the surface of $NaYF_4$:Ho^{3+}/Gd^{3+} NPs through two binding strategies. Two kinds of Dye molecules, i.e., Perylene Propionic Acid (PPA_2) and Commercial Coumarin (CC), were used to explore the binding procedures by altering the mass ratio of Dye molecules over NPs from 1:300, to 1:200, and to 1:100. It was observed that the UC intensity for a hybrid nanomaterial was enhanced relatively to bare $NaYF_4$:Ho^{3+}/Gd^{3+} NPs. Amongst the mass ratios 1:100 exhibits the most optimal blue-to-UVB UC efficiency. In addition, proofs of the efficient sensitization of Dye antenna was acquired by the time-resolved spectra, the overlap of excitation and absorption spectra of bare NPs, free Dye molecules and the hybrid nanomaterials.

Chapter 1: Introduction

1.1 Phototherapy

The positive effects of sunlight to cure skin disorders had already been noticed in ancient times [3][8]. Psoriasis is a skin disorder, that manifests itself through plagues built by skin cells and consequently multiplies very fast [9]. Light therapy has been used as predominant treatment modality and keeps the scepter among other alternative ways of treatment because it is affordable and meanwhile provides a good balance between the negative side effects and the effectiveness to cure the symptoms [3][1].

Sunlight is known to contain ultraviolet (UV) spectrum, which can be further classified into UV-A (320nm -400 nm), UV-B (290nm -320 nm) and UV-C (200nm-290 nm) [3][9]. Except the UV-C, light in the UV-A and UV-B can reach the surface of the earth[9]. On the other hand, nowadays in the field of phototherapy narrowband UV-B (~311-313nm) is used as artificial light source to cure psoriasis[1].

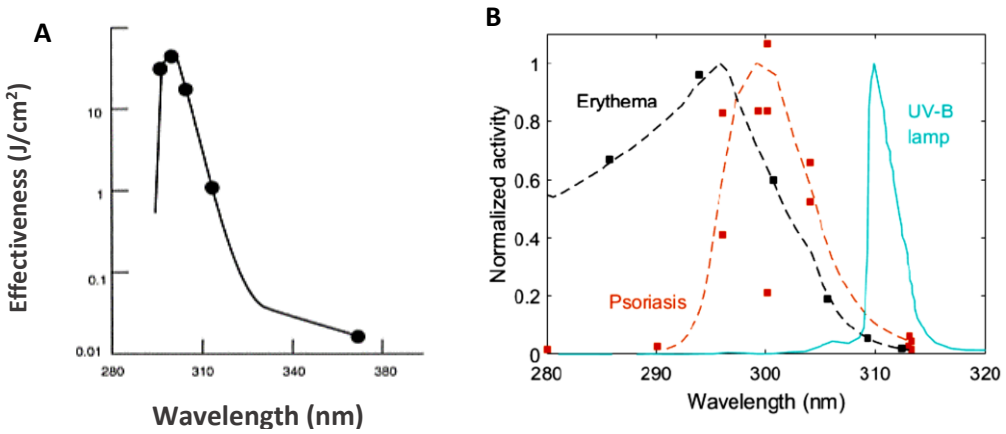

Figure 1.1. (A) Action spectrum for treatment of psoriasis. [A*dapted form Parish J.A., The science of photomedicine, Plenum Press, New York, 1982*]

(B) Action Spectra of Erytherma (black) and Psoriasis (orange) as well as a typical emission spectrum of UV-B Lamp (blue). The squares represent the values from experimental data, and dashed lines are plotted as a guide for the eye. *[Adapted from action spectrum for phototherapy of psoriasis, Parish JA, J Invest Dermatol, 76, (1981),359-362]*

Figure 1.1A illustrates the action spectrum of the annihilation of psoriasis [9].In that spectrum, the abscissa represents the different UV radiation wavelengths and the ordinate the effectiveness. The spectrum reveals that the maximum level of effectiveness for psoriasis treatment is at around 295nm-310 nm. At longer wavelengths a sharp decrease in the effectiveness is observed, such as the around 370 nm[10]. According to the spectrum in Fig. 1.1A, the most effective wavelength is at around 310nm[10]. Figure 1.1B illustrates the action spectra of Erythema (Sun Burn) and Psoriasis together with a typical spectrum of UV-B Lamp, respectively. The UV-B Lamp is characterized by a narrowband spectrum in about 311nm-313 nm. A direct comparison among these spectra reveals that the UV-B wavelength around 310 nm would balance the reduced detrimental 'sun burn' effects and the still provide sufficient effectiveness on curing the psoriasis disease. Commercial UV-B lamp is well designed for treatment of skin psoriasis [8] and do offer a permanent treatment for skin disorder.

However, when there are several affected areas that need to be treated for a patient, inevitable side effects will be caused within the light therapy treatment using NB UV-B lamp due to light spill[8]. That is, the healthy skins surrounding the disease area would be burned under overexposure of a NB UV-B lamp[8].

Additionally many hospital visits are necessary during the long time treatment plans [3][1], which will cause time consuming sessions and inabilities of the patients to perform the treatment by themselves. In an effort to eliminate all these disadvantages but to take advantage of the merits we propose an alternative phototherapy treatment method based on creation of novel blue-to-UVB UC by the field of spectroscopy.

1.2 Blue to UV-B Upconversion

Upconversion is a famous anti-Stokes luminescence process, through which, in principle, the absorption of 2 or more low-energy photons leads to emission of 1 high-energy photon[11][5] Through usage of dopant type and concentrations, dopants pairing styles, (nano-)crystal structure ,etc, UC of IR-to-NIR/visible and NIR-to-visible/UV have been reported for potential applications covering from lighting, display, to sensoring and biological imaging[12].

Lanthanide doped inorganic materials are best among all the reported upconverting systems, where hexagonal $NaYF_4$ host is famous for its benefits for efficient UC luminescence[13][14][15], and a maximum UC quantum yield of 12% was reported for the Gd_2O_2S:10%Er^{3+} phosphors[5]. New upconverting materials of Y_2O_3:RE^{3+}, Gd^{3+} and $NaYF_4$:RE^{3+}, Gd^{3+} (RE = Er, Tm, Dy, Ho) were prepared by our group with detectable blue-to-UVB UC luminescence. Through analysis using an OPO pulsed laser and a CW laser, optimized UC systems were further obtained to be Y_2O_3: 1%Ho^{3+},10%Gd^{3+} and $NaYF_4$:1%Ho^{3+},25%Gd^{3+}, respectively. Although, this trigger promises to application of topical phototherapy, the weak absorption of intra-4f transitions of Ho^{3+} would be an intrinsic restriction to the practice. Efficient visible-to-UV UC is not so much explored and announced[16] and also there are no reports for exploration in blue (~450 nm)-to-UVB (~312 nm) UC. The earliest Dye -sensitized NIR-to-visible upconverting nanoparticles was reported in 2012 by Hummelen group[6], where a very high enhancement of UC intensity was achieved due to efficient FRET from Dye antenna to Yb^{3+} ions.

1.3 Aim of the Project

The aim of this project is to explore, to realize and optimize Dye -sensitized blue-to-UVB UC luminescence in hybrid nanomaterials, where Dye molecules act as antennas surrounding the core $NaYF_4$:Ho^{3+}, Gd^{3+} nano-upconverters. Dye molecules that were used in this study intensively absorb the blue photons in a broad range (Fig. 1.2) and then resonantly transfer energy to the conjugated Ho^{3+} sites (see the spectral overlap in Fig. 1.2). Ideal results would be sufficient UV-B UC from the hybrid nanomaterials, for the phototherapy treatment of skin disorders, under a low-power ordinary blue LEDs source.

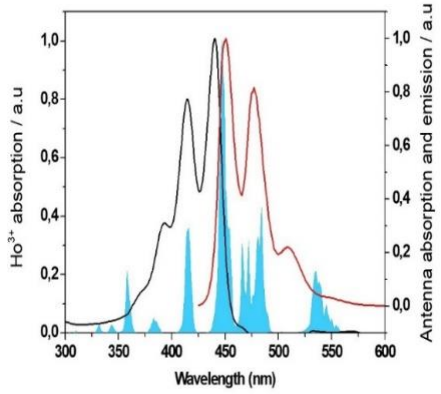

Figure 1.2: Absorption and emission spectra of PPA_2 (black and red line respectively) combined with absorption spectrum of Ho^{3+}(blue lines). The wavelengths in which all of them are crossed, is suitable for trap of the photons from the antenna and subsequently transfer it to Ho^{3+} sites.

In this current project, the exploration will comprise three main steps (Fig. 1.3):

I. The first step is to synthesize batches of $NaYF_4$:x%Ho^{3+},25%Gd^{3+} (x= 1, 3, 5, 8, 10) and $NaYF_4$ NPs for comparison of energy quenching effects by pure sensitization.

II. The second step is to replace the existing Oleate ligands on the surface of the NPs with Dye antennas. This attachment process will be performed through two exchange methods using two kinds of Dye molecules, i.e, PPA_2 and CC (Chapter 3).

III. The last experimental step, also the main challenge of this study, is to find the optimal weight ratio between the Dye molecules and the co-doped NPs in the hybrid upconverting nanomaterials. Practically the balance only can be found with a plenty of comparable lab works to optimize the mass ratio of Dye molecules over the NPs.

Undoubtedly more Dye molecules will result stronger absorption to blue light, but usually concentration quenching of the Dyes easily happen to lower the energy transferred to the Ho^{3+} sites, as well as the luminescence efficiency.

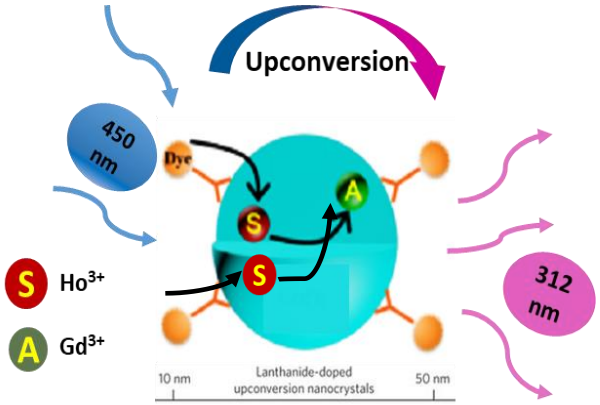

Figure 1.3: Dye sensitization and upconversion (UC) from blue(450nm) to UV-B (310m).NPs are doped with two different Ln^{3+} ions (Ho^{3+} and Gd^{3+}). Two independent Ho^{3+} ions absorb the blue light by means of an energy transfer from attached Dye molecules). The added up energy is transferred to a nearby Gd^{3+} ion, which finally emits UV-B UC luminescence.

Chapter 2: Theory

2.1 Luminescence

Luminescence is a process in which electromagnetic radiation is emitted after absorption of any form of sufficient excitation energy. The electrons of a luminescent entity are raised to an excited state and emit electromagnetic radiation while returning to back to their original state. Sometimes the return to the ground state can have many intermediate steps both radiative and non-radiative. The emitted electromagnetic radiation can be in the spectral region of the ultraviolet, visible or infrared [17].

In our case we focus on photoluminescence of upconverting the absorbed visible photons to UV-B photon re-emitted. Inorganic materials are widely used phosphors because of their stable chemical and physical properties, as well as their ability to host Lanthanide dopant ions for colourful photoluminescence[17] The context of this thesis, it will be focussed on photoluminescence and to the dominant role of Gd^{3+} within this project, the main interest lies in the unique emission in the ultraviolet spectral region[17].

2.2 Energy Levels of Lanthanide ions

Lanthanide elements or Rare Earth (RE) elements were discovered between 18th and 20th century and their name was an outcome of their difficult chemical extraction from the earth and of their limited abundance in nature compared to the most abundant element on earth silicon. They are placed in the first row of the f-block elements at the bottom of the periodic table and are Y, Sc, La, Ce, Pr, Nd, Pm, Sm, Eu, Gd, Tb, Dy, Ho, Er, Tm, Yb, and Lu. Their electronic configuration in the ground state is **$4f^n$ $5s^2$ $5p^6$**(or **[Xe] $4f^n$** (with n taking values between 0 and 14) [18][19].

Lanthanide ions are most stable in a trivalent oxidation state (Ln^{3+}). Even though they are intentionally doped as impurities in the material they are placed, they form optically active centres and are important for the photoluminescence [18].

This study utilizes intra-configurational 4f-4f transitions, which are located in the UV-Vis and NIR range for trivalent lanthanides. They are characterized by narrow emission bands. This is an outcome of the partially 4f shell and the fact that 4f electrons are shielded from the outer chemical environment of 5s and 5p electrons [20].

Due to the mutual interaction of the different 4f electrons, the $4f^n$ configuration of Ln^{3+} ions splits into different electronic levels. These interactions are described by the following phenomenological Hamiltonian (Formula 2.1) [18][21]:

$$H = H_0 + H_{\mathrm{el-el}} + H_{\mathrm{so}} + H_{\mathrm{cf}} \quad \textbf{(2.1)}$$

H_o: Hamiltonian in the central field approximation
$H_{el\text{-}el}$: Electron-electron interaction (due to mutual repulsion of electrons)
H_{so}: Spin-orbit interaction (coupling between spin and orbital angular momentum)
H_{cf}: Crystal field interaction (due to the crystal field of the host matrix)

The energy levels of the different 4f orbitals are split and result in a rich energy level landscape for each trivalent lanthanide ion. Due to the shielded character of the 4f orbitals, the energy of the various levels is almost independent from the embedding host compound and thus, allows for a collection of the various energy levels for each lanthanide. The corresponding scheme for the trivalent lanthanide ions is called the Dieke diagram (Appendix 1). The width of the lines depicted in this diagram provides information on the order of magnitude of crystal field splitting [22][23] [24].

2.3 Quantum Numbers and Term Symbols

The electronic structure of atoms is superficially described by their electronic configuration. This is, however, not a complete description of the arrangement of the electrons in atoms[25].

A configuration contains several electronic energy states, each of them can be described from the following set of Quantum numbers [20][26]: (i)**Principal quantum number (*n*)** (size of the orbital) ,(ii)**Azimuthal (Orbital angular momentum) quantum number** $(\boldsymbol{l})$ (shape of the orbitals) (iii)**Magnetic orbital angular momentum quantum number** $(\boldsymbol{m_l})$ (spatial orientation of an orbital, orbital magnetic moment) and (iv)**Magnetic spin quantum number** $(\boldsymbol{m_s})$ (spin projection of the electron, spin magnetic moment)

Microstates account for the fact that different occupation patterns of the electrons in orbitals may lead to different energies due to the mutual electron repulsion[25]. The total number of microstates for *x* electrons divided over the 7 4f orbitals each allowing for the occupation by two electrons with differing m_s quantum number is given by (14!/[*x*!(14-*x*)!]. It should be noted that several of the microstates may still be degenerate, i.e. have the same energy. Microstates can be labelled by term symbols [23].

A term symbol **($^{2S+1}L_J$)** is a combination of letters and numbers used to classify the microstates of a many-electron system by means of its angular momentum quantum numbers[26][27].

***L*:** Total orbital angular momentum
2*S*+1: Spin multiplicity
***J*:** Total angular momentum

According to the Clebsch-Gordan series (Formula 2.2), the sum of all individual angular momenta $\boldsymbol{l}$ of the electrons represents the magnitude of the angular momentum known as total orbital angular momentum (***L***). Exemplarily, for two electrons, the allowed values of *L* are given by

$$L = l_1 + l_2,\ l_1+l_2-1,\ldots,\ |l_1-l_2| \qquad (2.2)$$

The maximum value is obtained when two orbital momenta have the same direction ($L=l_1+l_2$) and the minimum when the momenta have opposite directions ($L=|l_1 - l_2|$). The representation of the *L* values into alphabetical letters is compiled in Table 2.1[26][27].

Table 2.1: Total orbital angular momentum labelling with capital letters for term symbols[26][27]**.**

L	**0**	**1**	**2**	**3**
Letter	**S**	**P**	**D**	**F**

The multiplicity **2*S*+1** describes the various degenerate spin projections characterized by M_S for a given total spin *S* quantum number. This degeneracy only gets lifted in the presence of an external magnetic field (Zeeman effect).

As an angular momentum, it can also be constructed from the different electron contributions by the Clebsch-Gordan series. For the example of two electrons, it[26][27]:

$$S = s_1+s_2,\ s_1+s_2-1,\ldots,\ |s_1-s_2| \qquad (2.3)$$

A single electron has a m_s value of +1/2 if the electron spin is up and m_s value of -1/2 if the electron spin is down. Consequently, a pair of electrons with opposite spins has a total *S* = 0.

The total angular momentum *J* is described by the quantum number *J* and gives information about coupling between spin and orbital angular momentum of a multielectron system[28].

According to Clebsch-Gordan series, the total angular momentum is defined as[28]:

$$J = L+S, L+S-1,\ldots., |L+S| \qquad \textbf{(2.4)}$$

In order to study the possible transitions of the lanthanide ions between the energy levels after their excitation, it is first necessary to determine the original ground level.

To determine the term that corresponds to the ground state configuration, Hund's rules may be used, that read as follows(Fig.2.1) [26][27][28]:

i. The terms with highest spin multiplicity $2S+1$ describes the ground spin multiplicity

ii. For terms with the same maximum spin multiplicity, the terms with highest L value are lower in energy.

iii. For terms with maximum spin multiplicity and L, it has to be distinguished between less or more than half-filled shells. If the shells of the atom are less than half-filled the lowest value of J affords the ground level. If the shells of the atom are more than half-filled the highest value of J gives the ground level instead[26][27][28].

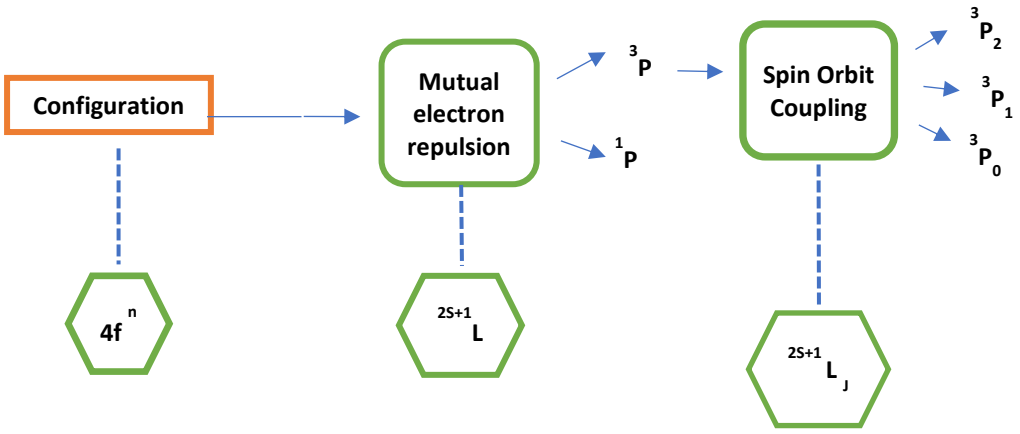

Figure 2.1: Illustration of the interactions that lead to energy level splitting .and what kind of information convey each interaction[26][27][28]

2.4 Allowed or Forbidden Optical Transitions

Not every imaginable transition necessarily occurs. Spectroscopic selection rules that can be derived from quantum mechanics, actually define if transitions are allowed or forbidden. The two most prominent rules are the spin selection rule and the Laporte selection rule (parity selection rule)[17][25].

i. Spin selection Rule: During a transition, spin must be conserved ($\Delta S = 0$). For spin conservation, the corresponding emission transition is referred to as fluorescence, while for a spin flip ($\Delta S \neq 0$), it is referred to as phosphorescence.

ii. Laporte selection rule: Electric-dipole transitions are forbidden between levels of the same parity (e.g. 4f-4f electric-dipole transitions are not allowed).

In contrast to electric dipole transitions, magnetic dipole or electric quadrupole radiation are allowed within the 4f shell. Table 2.2 includes the three main categories of transitions for lanthanide ions together with the resulting selection rules on the angular momentum quantum numbers[18].

Table 2.2: Transitions and values of S,L,J calculated based on the selection rules[18].

Transition Mechanism	S	L	J
Electric Dipole [ED]	ΔS=0	ΔL=0,±1	ΔJ=0,±1
Magnetic Dipole [MD]	ΔS=0	ΔL=0	ΔJ=0,±1
Electric Quadrupole [EQ]	ΔS=0	ΔL=0,±1,±2	ΔJ=0,±1,±2

2.5 Energy Transfer Mechanisms

Energy transfer can happen when the resonance condition and the Förster Resonance Energy Transfer model are fulfilled. The overlap between the emission spectra of donor and the absorption spectra of acceptor prove the existence of the resonance condition[17].

The possible energy transfers from an excited ion (donor) to an acceptor ion are [29]:

i. **Resonant Radiative transfer:** According to this type of energy transfer acceptor ions that are within a photon distance absorb photons emitted by donor ions
ii. **Resonant non-Radiative transfer:** In the non-radiative transfer no emission of the donor is observed because its excitation is transferred to the acceptor before a quantum of fluorescence is emitted (van der Waals type coulomb interactions)
iii. **Phonon assisted non-Radiative transfer**: There is an energy mismatch (ε) between the donor and the acceptor, which can be compensated with the vibration energies of local and lattice modes.
iv. **Cross Relaxation:** A case of non-radiative transfer that happens between two ions. If the energy levels of the two ions are identical diffusion process takes places. If the energy levels of the two ions are not the same self-quenching takes place.

Förster Resonance Energy Transfer (FRET) describes the energy transfer from a donor the an acceptor (Resonant non-Radiative transfer)(2.5)[17][18][30].

$$S^* + A \rightarrow S + A^* \quad \textbf{(2.5)}$$

S: sensitizer or donor
A: activator or acceptor
*: excited centre

Based on quantum mechanical theory and dipole-dipole interactions, Förster thought that the interactions will be stronger if both electric dipole transitions are allowed. The interaction energy will be proportional to the inverse of the third power of the interionic distance. The equation 2.6 calculates the transfer probability [29].

$$\boldsymbol{P_{SA} = \frac{2\pi}{h} |\langle S^* A^0 | H_{SA} | S^0 A^* \rangle|^2 \rho_E} \quad \textbf{(2.6)}$$

$\boldsymbol{P_{SA}}$**:** Transfer probability
$\mathbf{H_{AS}}$: Electric dipole-dipole interaction Hamiltonian and
$\boldsymbol{\rho_E}$: Density of states by the vibrations

The equation can also be given by the following equation 2.7[29][31].

$$P_{SA} = \frac{1}{\tau_s}\left(\frac{R_0}{R}\right)^6 \quad \textbf{(2.7)}$$

$\boldsymbol{\tau_s}$**:** Lifetime of the sensitizer in the excited state (multiphonon radiative decay is included)
$\mathbf{R_0}$: Critical distance for which excitation transfer and spontaneous deactivation of the sensitizer have equal probability.

$\mathbf{R_0}$ can be experimentally obtained from spectroscopic data through $\mathbf{R_0^6} = \frac{9ln10}{128\pi^5}\cdot\frac{K^2}{n^4} * \gamma_D * J$

In our study Ho^{3+} ions will be the absorber, and then an UV-excited Ho^{3+} ion will act as donor ion to resonantly transfer its energy to a nearby Gd^{3+} acceptor ion. Although complete resonant non-radiative transfer was desired, in some cases Ho^{3+} ions made cross relaxation transitions, and hence quenched emission bands were recorded.

2.6 Upconversion Mechanisms

Upconversion (UC) is a way for energy transfer among the Ln^{3+} and is an optical process where the energies of two or more photons were added up to create another photon re-emitted at higher energy. Ground state of an ion can be excited to a higher energy level through radiation absorption and via a dipole-dipole resonant interaction they can transfer their energy to acceptor ions. UC emission occurs from the acceptor ion when it goes back to its original ground state [32][17]. The emissions are detectable from near infrared (NIR) to visible or ultraviolet spectral region[13][32].
There are six known two-photon UC processes (Fig.2.2), [17][29]:

i. **APTE (Addition de Photon par Transferts d'Energie) effect or Energy transfer Upconverion (ETU):** Ions A transfer energy to ion B. Ion B goes to higher energy level and emits higher energy level while going back to its original ground state
ii. **Excited State Absorption (ESA):** Energy is absorbed in two steps by only one ion
iii. **Cooperative sensitization**: Ion B which has no initial energy, is excited from two ions A at the same time and emits radiation from a higher energy level with no intermediate steps.
iv. **Cooperative luminescence:** The energy of two ions A is combined to one higher level quantum
v. **Second Harmonic generation (SHG)**: The frequency f is doubled with no intermediate steps of absorption (frequency doubling)
vi. **Two photon absorption:** Two photons were absorbed the same time and there are no steps between the different states. Radiation is emitted by one photon

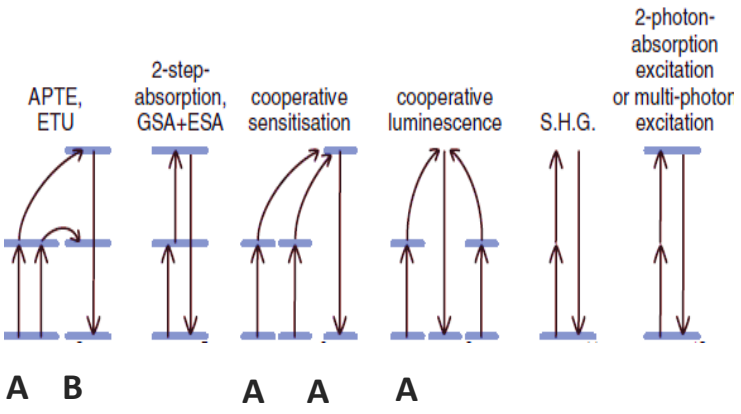

Figure 2.2: Schematic representations of six UC processes which described extensively [13].

All UC mechanisms are listed according to their efficiency on Table 2.3. APTE seems to be the most efficient UC process[17].

Table 2.3: Efficiency of each process of Fig. 2.2. The incident power was 1 Wcm^{-2}[17]

Mechanism	Efficiency
Sequential energy transfer (APTE or ETU)	**10^{-3}**
Two-step absorption	**10^{-5}**
Cooperative sensitization	**10^{-6}**
Cooperative luminescence	**10^{-8}**
Second Harmonic generation	**10^{-11}**
Two-photon excitation	**10^{-13}**

Even though APTE effect (or ETU) is the most efficient process there are certain requirements to be fulfilled necessarily. The sum up energy of ions A (donor) must be of almost the same with the this of ion B (acceptor) (resonance condition), and the space between the ions A and B should meet with FRET model (see section 2.5)[24].

It was proved by Pollnau et al.[33] that the UC emission Intensity I^{em} is proportional to nth power (n= #of photons absorbed/upconverted photon emitted) of the pump power P (2.8)[33].

$$\boldsymbol{I \propto P^n} \quad \textbf{(2.8)}$$

For the ETU process, Blue light (λ_{ex}=450nm) is used as exciting radiation for the two Ho^{3+} ions, which transit from their ground state $^5I_8$ to an excited state of $^5F_3$ or $^5S_2$. At these energy states the two Ho^{3+} ions cooperate in a way that they sum up their energy in one of the two Ho^{3+} ions. Following, the Ho^{3+} ion has the total energy occupying UV-excited $^3M_{10}$ state (or the state slightly below due to fast nonradiative decay) (Fig. 2.3).
FRET will work from the excited Ho^{3+} ion to one nearby Gd^{3+}, mainly exciting ^6P_j states. Finally, the excited ^6P_j states was decayed to the $^8S_{7/2}$ state by efficient UV-B emission at around 310 nm. Notice that Gd^{3+} is a perfect candidate for skin psoriasis treatment due to its unique UV-excited state of ^6P_J lying around 32000 cm^{-1} rather efficient for UV-B emission at about 312 nm[17]**.**

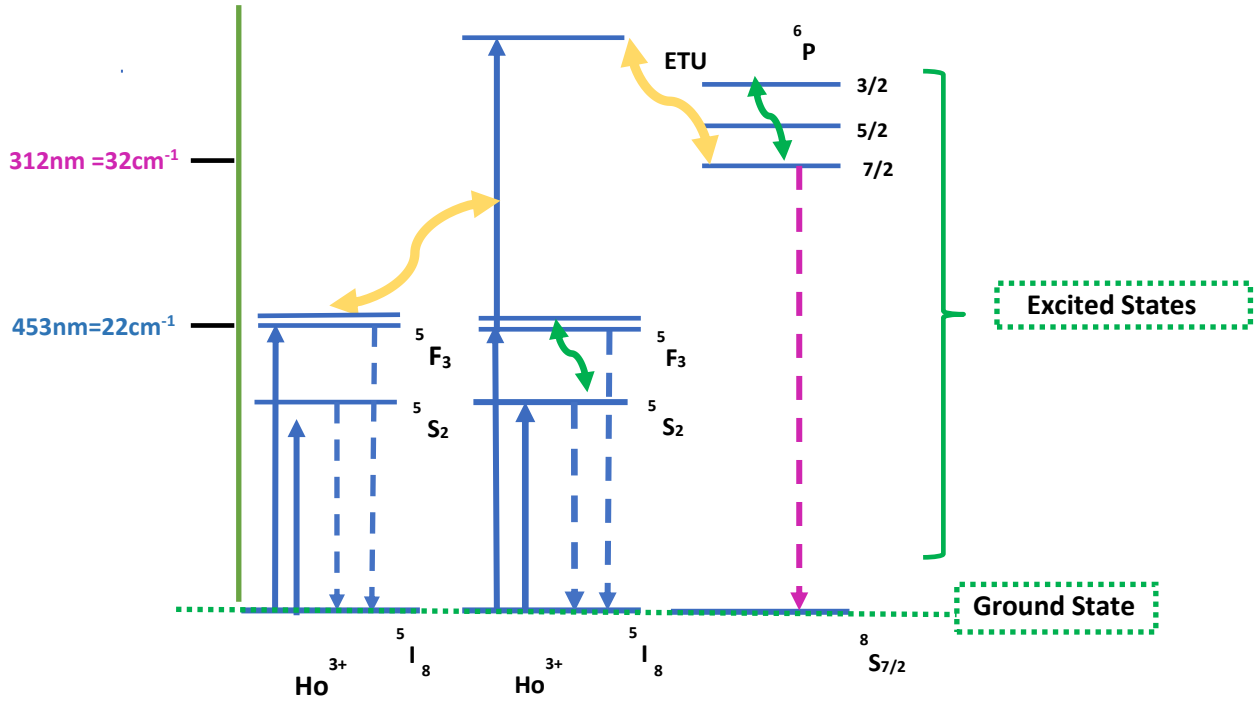

Figure 2.3: Total UC mechanism between lanthanide ions. In the first step incident Blue light is absorbed from two Ho^{3+} lanthanide ions and transferred to one Gd^{3+} ion from which radiative emission at 312nm occurs. Non-radiative processes which result in quenched UC emission intensity are depicted with green. ETU is represented with the yellow arrows.

2.7. Non-Radiative processes

As referred in section 2.6 the UC process of Ln^{3+} ions consists of three steps, but non-radiative processes such as cross relaxation(section 2.5), back energy transfer and non-radiative decay would be detrimental to the efficiency of UC process [34].

Back energy transfer can occur from the acceptor ion (here Gd^{3+}) to donor ion (here Ho^{3+}) if there exist relatively stable intermediate levels for acceptor that quite approximate to the levels of donor ion. Especially in the case of heavily doped donor, the back energy transfer will become much more efficient, which might severely decrease the efficiency of an desired UC luminescence.[35] Such process in this study will be distinguished through lifetime measurements in Chapter 4.

The definition of phonon energy corresponds to the energy difference between two electronic states. During multiphonon relaxation, the excited energy of Ln^{3+} ions goes down from a high energy state to a lower energy state without radiative emission. The non-radiative energy is dispersed by lattice vibrations in the crystals, rate of which is faster than radiative decay rate [23][36].

Overall non-radiative processes are an outcome of ion-phonon interactions and can be characterized by a relaxation rate. The energy difference between the electronic states, the temperature and the frequencies of the vibration modes can affect the rate of multiphonon relaxation (2.10)[37][36].

$$W(T) = W(0)\left[\frac{\exp(\frac{h\nu_m}{kT})}{\exp(\frac{h\nu_m}{k})-1}\right]^{\frac{\Delta E}{h\nu_m}} \qquad (2.9)$$

$\boldsymbol{W(T)}$**:** Multiphonon relaxation rate
$\boldsymbol{h\nu_m}$: Maximum phonon energy of the lattice vibrations
$\boldsymbol{\Delta E}$: Energy difference between the adjacent energy states
$\boldsymbol{W(0)}$: Spontaneous transition rate when the phonon modes are in their ground state for T=0K[36][38]

To eliminate the undesirable non-radiative relaxation host lattices with low phonon energy play an effective role, which therefore mainly results in the employment of $NaYF_4$ ($350cm^{-1}$) as a host matrix in our experiments.[19][39][40].

2.8 Decay Curves

Decay curves are typically acquired to show the time that a photon needs to return to from an excited to the ground state. This can happen with radiative or non-radiative way. Decay time is usually obtained by fitting the measured decay curve to an exponential or multi-exponential functions. A severe non-radiative process makes decay time shorter, and further decrease the luminescence efficiency. In this study Decay curves were recorded at 310 nm for Gd^{3+} UV-B emission) and at 500 nm for emission from Dye molecules [41]. It should be noted that high doping levels can lead to destructive cross relaxation. An indisputable proof about presence of cross relaxation is the shortened lifetime and the decreased luminescence intensity [42][43].

The Average lifetime can be calculated from the formula 2.10 [41]:

$$\tilde{\tau} = \frac{\sum_i a_i \ \tau_i^{\ 2}}{\sum_i a_i \ \tau_i} \quad (2.10)$$

$\boldsymbol{a_i}$ **:** Amplitude
$\boldsymbol{\tau_i}$: Decay time of the individual components for multi-exponential decay profiles

2.9 Energy Transfer from Dye Molecule to Core $NaYF_4$-NPs

In the current study, in order to increase the UC intensity of Gd^{3+}/Ho^{3+} co-doped NPs organic Dye molecules, namely PPA_2 and CC, were specially designed, and employed as antennas on the surface of NPs. The designed Dye molecules would have quite intense broadband absorption (in principle absorption section of Dye molecules would be more than 1000 times as that of intra-4f transitions of Ho^{3+} ions), and can efficiently trap blue photons around 450 nm (Fig.2.5A)and excited to S_1 energy level[44][45]. Through a well-known FRET process the excited Dye dangling can efficiently sensitize the nearby Ho^{3+} ions on the surface of NPs (Fig. 2.5B). The 'added-up' energy of two blue-excited Ho^{3+} ions will finally result in the efficient population of Ho^{3+} UV-excited states, and subsequent energy transfer to nearby Gd^{3+} into ^6P_J states for UV-B emission at about 311nm-313nm (Fig. 2.5C)[46].

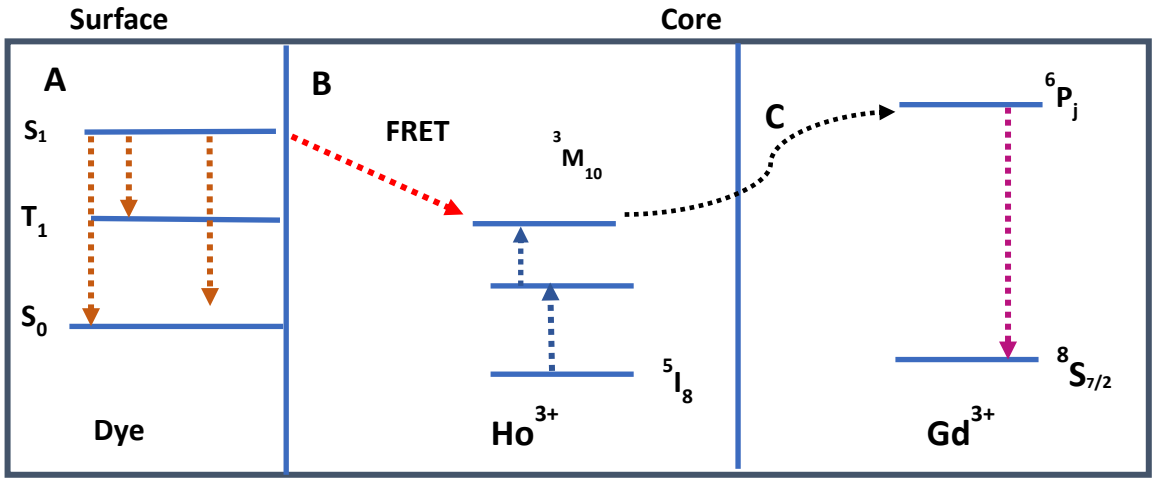

Figure 2.4: Energy transfer from the antenna molecule to Ho^{3+} and from Ho $^{3+}$ to Gd $^{3+}$. S_0 is the ground state, S_1 excited state. Energy transfer to trivalent lanthanide ion (red arrow) takes place through Forster Resonance Energy Transfer (FRET). Black dot arrow represent the Upconversion (UC) mechanism between trivalent lanthanide ions.

Such hybrid system allows us to optimize the sensitization effects by varying the distance between Dye molecules and Ln^{3+} sites, as well as the number of Dye molecule dangling on the surface of NPs. For the sake of purpose, the different mass ratios of Dye molecules over NPs were employed by us in different hybrid upconverting nanomaterials.

Chapter 3: Materials and Methods

This chapter will provide an overview of two different methods used for the synthesis of β-$NaYF_4$ NPs and two processes used for the conjugation of antennas on UCNPs. Different characterization techniques were employed to prove the Dye sensitization, the enhanced UCL and the loss pathways that compete with UCL.

3.1 Synthesis of $NaYF_4$:25%Gd^{3+}, x%Ho^{3+} -NPs

3.1.1 Chemicals

Table 3.1 summarizes all chemical compounds which are necessary for the conduction of the experiments. All chemicals are used without further purification.

Table 3.1: Summary of the chemical compounds used in the experiments.

Name	Formula	Purity	Manufacturer
Oleic Acid	**OA**	**90%**	**Sigma-Aldrich**
1-Octadecene	**ODE**	**90%**	**Sigma-Aldrich**
Cyclohexane	**CH**	**99.5%**	**Sigma-Aldrich**
Ethanol	**EtOH**	**99.8%**	**Sigma-Aldrich**
Methanol	**MeOH**	**99.85%**	**Sigma-Aldrich**
Sodium Hydroxide	**NaOH**	**>97%,**	**Sigma-Aldrich**
Ammonium Fluoride	**NH_4F**	**>98%**	**Sigma-Aldrich**
Gadolinium Acetate Hydrate	**$Gd(Ac)_3.H_2O$**	**99.9%,**	**Sigma-Aldrich**
Holmium Acetate Hydrate	**$Ho(Ac)_3.H_2O$**	**99.9%**	**Sigma-Aldrich**
Yttrium Acetate Hydrate	**$Y(Ac)_3.H_2O$**	**99.9%**	**Sigma-Aldrich**
Tetrahydrofuran (without stabilizer)	**THF**	**99,9%**	**Sigma-Aldrich**
Gadolinium Chloride Hexahydrate	**$GdCl_3.6H_2O$**	**99.9%**	**Sigma-Aldrich**
Holmium Chloride Hexahydrate	**$HoCl_3.6H_2O$**	**99.9%**	**Sigma-Aldrich**
Yttrium Chloride Hexahydrate	**$YCl_3.6H_2O$**	**99.9%**	**Sigma-Aldrich**
N,N-Dimethylformamide(anhydrous)	**DMF**	**99.8%**	**Sigma-Aldrich**

3.1.2 Methods for synthesis of Bare $NaYF_4$ NPs

It is known that $NaYF_4$ nanocrystals have two phases: the cubic α-phase and the hexagonal β-phase [47].Based on the experimental studies of Haase et al [47] which focused on $NaYF_4$-based UC nanocrystals, as well as the studies of Geitenbeek et al. [48] which increased the number of ligands bound on the surface of nanoparticles and on Wang et al[49]. In this project β-$NaYF_4$:25%Gd^{3+},x%Ho^{3+}-NPs (here abbreviated as **x%Ho^{3+}-NPs**) were synthesized. The preparation of NPs was conducted in two steps; the nucleation and the growth of the NPs. This synthesis is known as co-precipitation method [48].

In the current study two different methods were used for the synthesis of β-$NaYF_4$:25%Gd^{3+}, x%Ho^{3+} -NPs. Standard Schlenkline techniques in dry glassware were used in both of them.

Method 1

In this method the synthesis of 1 mmol hexagonal β-phase $NaYF_4$:10%Ho^{3+},25%Gd^{3+} NCs was based on acetate precursors and the starting materials were Gd $(Ac)_3.H_2O$ (~0,0835 gr), Y$(Ac)_3.H_2O$ (~ 0,1729 gr) and Ho$(Ac)_3.H_2O$(0,0342 gr), 6 ml OA and 12 ml ODE. These ingredients were added in a 50 ml three neck-round bottom flask which was connected to a Schlenk line. Under vigorous magnetic stirring the mixture started degassing and was gradually heated from RT up to 145 ^{0}C for at least 30 minutes (vacuum atmosphere). As a result, an optically transparent solution was formed.

In order to remove all residual water, the solution was flushed three times by switching the atmosphere from vacuum to N_2 gas. Then, the mixture was cooled down with gentle stirring from 145 ^{0}C to 30 ^{0}C under N_2 atmosphere.

2.5 mmol (~0.1 gr) NaOH and 4 mmol (~ 0,1481 gr) NH_4F were then added in 10 ml MeOH and the mixture was left for sonication for 1hr, in order to be completely dissolved. After sonication it was quickly injected (with syringe) into the reaction solution which was at RT and under N_2 atmosphere. The resultant white turbid reaction mixture was kept under vigorous magnetic stirring for 16hr (N_2 atmosphere). NaOH and NH_4F were kept in the cupboard of the lab so they were not totally dry. That means that some residual water during the synthesis may come from these ingredients.

Heating of the turbid solution under vacuum atmosphere from RT to 100^{0}C led to evaporation of all MeOH and resulted to a transparent solution (more than 30 minutes). The small nuclei small cubic $NaYF_4$ NPs became large hexagonal NPs by further heating of the transparent solution from RT to 300^{o}C for 2hrs. The resultant solution was then again cooled down to RT and it became slightly turbid with a yellowish colour. For the collection of the desired NPs and the removal of the excess reagents and solvents, the reaction mixture was washed several times[48][49].

Washing procedure

[1] One equivalent of EtOH was added and the mixture was centrifuged for 8 min. Removal of the supernatant.
[2] The resulting sediment was re-dispersed in 5 ml CH.
[3] The repetition of Step 2 is necessary so many times as needed in order to get an optically colorless CH solution with dispersed the desired NP's in a final concentration of 40 mg/ml.

Method 2

Method 2 was based on the same synthesis protocol 2 as Method 1 but with some adjustments. Specifically, when the temperature of the reaction mixture reached 145^{o}C it was left for stirring under vacuum for 50 min and then injection followed under N_2 atmosphere at 30^{0}C. The solution degassed for evaporation of MeOH up to 90^{0}C and up to 135^{0}C to remove all residual water. The atmosphere of the reaction mixture was switched to N_2 and immediately the solution was heated up to 300^{o}C for 2 hours. To keep the temperature stable at 300^{0}C aluminium foil was used to cover the three-neck flask which contains the reaction mixture. In the last step the solution was cooled down to RT and a yellowish transparent solution was obtained. The content of the flask was divided into three empty glass vials (40ml) for washing. The washing steps are described in detail in the following section. According to this experimental procedure, the synthesis of β- $NaYF_4$:x%Ho^{3+},25%Gd^{3+}NPs (x=1, 3, 5, 8, 10, 12) was achieved.

Washing Procedure

In order to know the exact amount of the NCs in the sediment of washing step [5], all the empty glass vials (40 ml) were weighed.

[1] Two equivalents of EtOH were added in each glass vial which contained the final reaction mixture. Centrifugation for 10-15 minutes (3100 rpm).
[2] Repetition of step but instead of EtOH mixture CH:MeOH: EtOH~1: 4:2.5 was used.
[3] The sediment was re-dispersed it in a total volume of 8 ml CH (approximately 3 ml in each glass vial). The mixture was centrifuged at 2400 rpm for 10min.
[4] The supernatant solution was then transferred in a 20 ml glass vial and 2 equivalents of EtOH were added. Centrifugation for 10 min (3000 rpm).
[5] The sediment was kept in the 20 ml glass vial according to the final concentration of the NPs ~ 40 mg/ml.

Method 2 has more advantages in comparison to Method 1. The NPs obtained from method 2 were much more and the quality of the NPs remained the same even though the duration of the synthesis was remarkably shorter (1 day including the washing steps) relative to Method 1 (2 days including the washing steps).

3.2 Binding Methods

As a next step the goal of this project was to enhance the UC intensity of the NPs. In order to accomplish PPA_2 Dye (Fig 3.1a) was used as an antenna because of its ability to strongly absorb the blue light around 450 nm and to efficiently emit photons around 470 nm by going through a quite small Stokes shift. In order to succeed the binding on the UCNPs surface the existing oleate ligands are replaced with PPA_2 Dye molecules through a process known as ligand exchange.

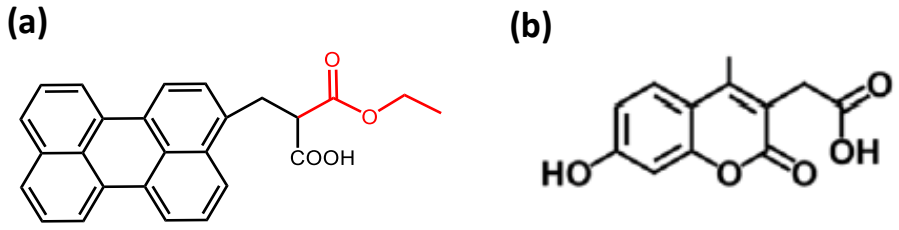

Figure 3.1: Molecular structures of: (a) PPA_2 Dye and (b) CC Dyes.

Two different binding methods were used in the current study:

Method A: Ligand Exchange via Direct Mixing Tetrahydrofuran (THF) solvent

The main advantage of this method is that there will be no loss of NPs through the procedure steps. The method is also very fast and the manipulation is easy. To optimize the binding on the surface of x%Ho^{3+}-NPs, PPA_2 Dye molecules are directly mixed with the NPs and THF was used as solvent. Different weight ratios of NPs: Dye were used in the experiments as presented on Table 3.2.

In these binding systems a fixed concentration of NPs (3 mg/ml) was used with a varying amount of PPA_2 Dye (stock solution of Dye: 0.1 mg/ml). Initially NPs (dispersed in CH) and Dye (bulk solution) were mixed in THF and left for stirring (1.5 hours) at RT. The Glass vials were continually covered with aluminium foil to prevent any possible light decomposition of the Dye or any influence happened by light during binding process.

Table 3.2: Different Systems (weight ratio) used, in order to optimize the most efficient Dye concentration. NPs concentration (3 mg/ml) and a total overall solution volume of 5 ml were standard.

System (NPs:PPA_2)	Total overall solution(ml)
1/100	5
1/200	5
1/300	5

Method B: $NOBF_4$ modification of NPs in DMF (N, N-Dimethylformamide) solvent

The experimental procedure of Wang [50] was referred so as to achieve a stronger Dye binding with the surface of NPs, in comparison to the direct mixing approach used in Method A.

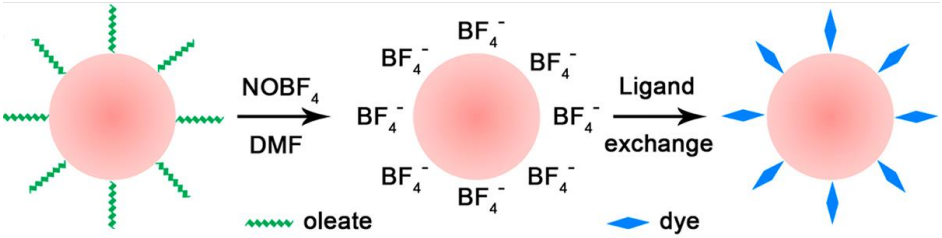

Figure 3.2: Steps followed to achieve ligand exchange using $NOBF_4$. In the first step Oleate ligands are substituted with BF_4^- in DMF and in the second step BF_4^- is exchanged with Dye molecules[50]

The Dye molecules used for this method was Commercial Coumarin (CC) Dye. In order to achieve CC-sensitized UCNPs, the first step was to exchange the oleate ligands with inorganic molecules BF_4^- and the second step was to substitute BF_4^- with CC Dye molecules (Fig. 3.2). The experimental procedure starts with the mixing of NPs in CH (40 mg/ml) with 5 ml $NOBF_4$ dissolved in CH_2Cl_2 (0.01 M) [50]. This mixture centrifuged for 10 minutes (3100 rpm). In order to get the UCNPs modified with $NOBF_4$, the sediment was washed with a weight ratio 1/1 of Hexane and Toluene and centrifuged for 20 minutes (3100 rpm). The precipitation dissolved in 5 ml DMF. Then this was mixed with CC bulk solution (1 mg/ml) in DMF. The weight ratios (PPA_2: Dye) whose optical properties where measured are those of table 3.2 [50].

The main reason for the use of a second binding method was that the $NOBF_4$ modification introduces strongest binding of the Dye on the surface of the UCNPs and it is irreversible in comparison to direct mixing.

3.3 Characterization

The success of the Dye binding on the NPs surface and the efficient energy transfer to the NPs were proved with spectroscopic explorations. Standard quartz cuvettes (2.5 ml) were used to measure the optical properties of the samples.

Absorption Spectra

The absorption spectra of free Dye and Dye sensitized NPs in different weight ratios were acquired with LAMBDA 950 UV-VIS-NIR Spectrometer (Perkin Elmer). The operating range of the instrument was 175-3300 nm.

Transmission Electron Microscopy (TEM)

The morphology and the size distribution of synthesized NPs were acquired with Transmission Electron Microscopy (TEM; Techai 10 Philips microscope).

Emission and Excitation Spectra

Emission and excitation Spectra were recorded using an Edinburgh FLS920 spectrofluorometer. Xenon Lamp 900 was the light source and R928 photomultiplier used as the photodetector.

Decay Curves

Decay Curves of Dye molecules were recorded with a picosecond (ps) pulsed diode Laser (λ_{ex}=405 nm), and decay curves of UV-B UC luminescence of active NPs were obtained using an OPO pulsed laser at 450 nm.

UV-B upconversion Measurements

Opolette laser was used as excitation source for the recording of the UC luminescence (λ_{ex}=450nm and λ_{em}= 310nm). In comparison with Xenon Lamp, OPO laser is stronger in power density and subsequently more suitable to realize blue-to-UVB UC luminescence that basically require high power excitation.

Continuous Wave (CW) Laser

An alternative laser to explore the UC luminescence of the Dye sensitized Gd^{3+}, Ho^{3+}: NPs is the continuous wave laser. This Laser is not so strong as OPO laser, and a detailed insight view of the two lasers is given in Chapter 4 of this study.

Chapter 4: Results and Discussion

This Chapter will provide information about the synthesized NPs. Mainly method 2(Chapter 3) was utilized because it is less time-consuming than Method 1 and gives the same efficiency and morphology results for the NPs

4.1 Characterization: Transmission Electron Microscopy (TEM)

The morphology and the size of the synthesized NPs were determined with the help of TEM images, through which the shape and the rough size of as-prepared NPs can be well known for a rigorous experimental comparison. In order to optimize the size and the shape of NPs three different strategies were followed. The first one was to synthesize NPs based on the effect of the use of two different precursors (chlorides and acetates) while keeping the quantity of all other ingredients constant.

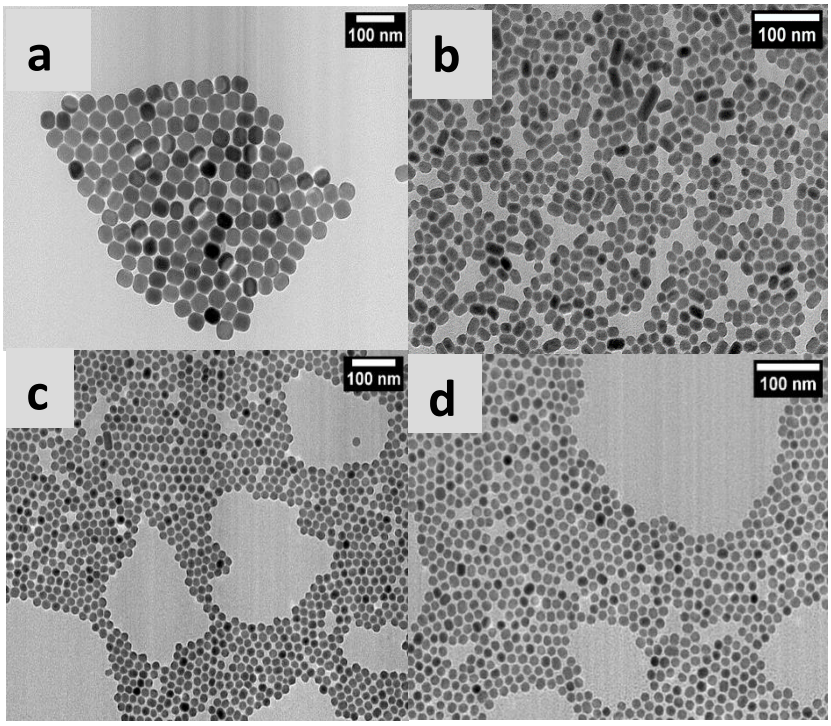

Figure 4.1: TEM images of samples with RE-chloride: (a) 3%Ho^{3+}-NPs, (c) 10%Ho^{3+}-NPs and RE-acetate: (b) 3%Ho^{3+}-NPs, (d) 10%Ho^{3+}-NPs

The size of the NPs was measured roughly using the scale bars of each TEM image which were acquired using a specially designed programme for TEM scaling bars. The size distribution of the NPs was determined after measuring 100 NPs in each TEM image. These results will provide quantitative analysis about of the effect of the NPs size within various binding systems. Images 4.1a and 4.1b represent the 3%Ho^{3+}-NPs that were synthesized with acetate and chloride precursors, respectively. In Fig. 4.1a where chloride precursor was used the sample shows homogeneous distribution of the NPs and the diameter of each NPs was estimated to be around 25±2 nm. In Fig. 4.1b, the NPs synthesized using the acetate precursor does not show homogeneous distribution with an estimated diameter around 15±2 nm. Summarizing, chloride precursor contributes to bigger NPs and more homogeneous distribution.

In order to gain insight of the effect of the precursors a second strategy which focused on synthesis of NPs with higher holmium concentration (10% Ho^{3+}) and with two different precursors was used (Fig. 4.1c and 4.1d). The samples in the TEM images display homogeneous distribution of the NPs.

The diameter of 10%Ho^{3+}NPs with chloride precursor is around 20±2 nm and those with acetate precursor around 16.5±2 nm. Even with the increase of the concentration of Ho^{3+}, RE-chloride NPs have bigger size and more homogeneous distribution compared to RE-acetate-induced NPs.

Comparisons were made among samples synthesized using same precursors but with different Ho^{3+} concentrations in order to check the effect of the concentration on the size and the shape of the NPs. To obtain this information the pairs of the TEM images of Fig. 4.1a and 4.1c and that of Fig. 4.1b and 4.1d comparing RE-chloride and RE-acetate precursor, respectively. In RE-chloride-induced samples the NPs have homogeneous distribution and the size decreases from 25±2 nm to 20±2 nm as the concentration of Ho^{3+} increases from 3% to 10%. In RE-acetate-induced samples the size distribution is not homogeneous, and the diameter of the NPs increases from 15±2nm to 16.5±2 nm as the concentration of Ho^{3+} increases from 3% to 10%. Therefore, based on the above three comparisons synthesis using chloride precursors offer better quality of NPs.

However, during the washing procedure there inevitably exist experimental difficulties to obtain an optically transparent colloidal solution of NPs in CH for RE-chlorides (Chapter 3). Finally, RE-acetate precursors have been chosen for the synthesis of the NPs in the following sections of this Chapter.

Synthesis of x%Ho^{3+} NPs using RE-acetate precursor

The last goal was to check the effect of the morphology and the size of the UCNPs synthesized using acetate precursors. The synthesis of x%Ho^{3+}-NPs (x=1, 3, 10) was performed and represented in Fig. 4.2a and c respectively. TEM 4.2d represent the inert $NaYF_4$ NPs without any lanthanide dopants. The shape of the samples was estimated in the same way as described for Fig.4.1.

The $NaYF_4$ NPs (Fig. 4.2d) show almost double the size in comparison to the other NPs (Fig. 4.2a-c). The NPs size for 1%Ho^{3+} is around 30±2 nm and for 20%Ho^{3+}NPs around 27±2 nm. In 4.2b the size of the NPs could not be measured because the NPs distribution was not homogeneous. It should be noted that the 4.1b and 4.2b TEM images came from the same batch of the NPs solution. This can be attributed to possible errors during the synthesis procedures such as in homogeneous temperature heating of the three-neck flask from the heating plate. Correspondingly, it can be concluded that the presence of lanthanide ions decrease the size of the NPs. Specifically, when the concentration of Ho^{3+} increases from 1 to 10%, there is a significant difference on the size of the NPs up to 3 nm.

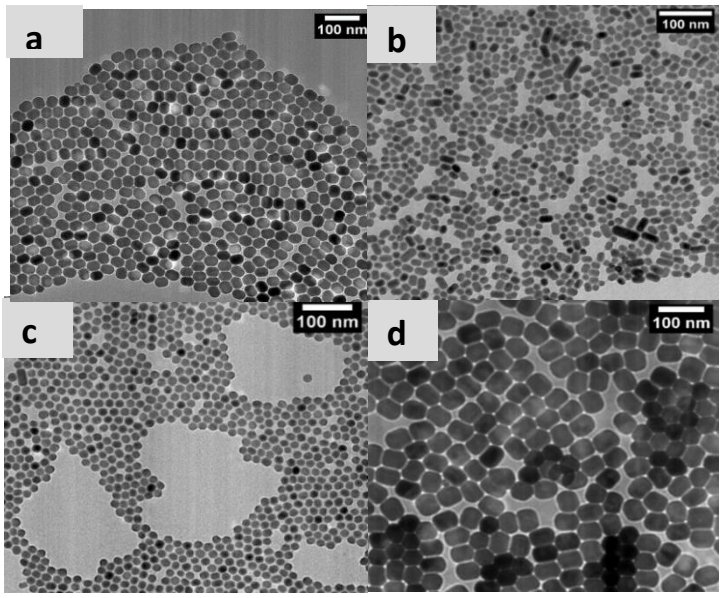

Figure 4.2: TEM Images of: x%Ho^{3+}-NPs prepared by RE-chlorides. (a-c) correspond to x=1, 3, 10 respectively and (d) $NaYF_4$ NPs.

4.2 Optical Absorption Spectra

Results for Direct Mixing of 10%Ho^{3+} -NPs (or $NaYF_4$-NPs) with PPA_2- Dye

The goal of this section was to measure and get results from the absorption bands of PPA_2 Dye molecules, the PPA_2 Dye sensitized inert NPs and the PPA_2 Dye sensitized active NPs. The Dye -bound UCNPs were constructed with direct mixing method. Table 4.1 contains the binding systems that were measured. The rows of the table contain the different samples that were used and the columns the samples that were measured in three different dilution levels.

Table 4.1: Samples that were synthesized for optimization of the best Dye concentration.

Dilution levels	x%Ho^{3+}-NPs:PPA_2	NaYF4 NPs:PPA_2	PPA_2
1:100	**x%Ho^{3+}-NPs: PPA_2**	**$NaYF_4$-NPs: PPA_2**	**Free PPA_2**
1:200	**x%Ho^{3+}-NPs: PPA_2**	**$NaYF_4$-NPs: PPA_2**	**Free PPA_2**
1:300	**x%Ho^{3+}-NPs: PPA_2**	**$NaYF_4$-NPs: PPA_2**	**Free PPA_2**

A fixed amount of 3 mg/ml of NPs (x%Ho^{3+}-NPs or $NaYF_4$-NPs) was used, while the amount of Dye changes according to the weight ratios of NPs:Dye ~ 1:100 (Dye ~ 30 µg/ml), 1:200 (Dye ~ 15 µg/ml) and 1:300 (Dye ~ 10 µg/ml). Furthermore, the free Dye molecules in THF (binding Method 1) solution were prepared with concentration 30, 15, and 10 µg/ml as blank references to the respective case of weight ratios of NPs:Dye. A UV-VIS spectrometer was used to acquire the absorption spectra represented in Fig. 4.3.

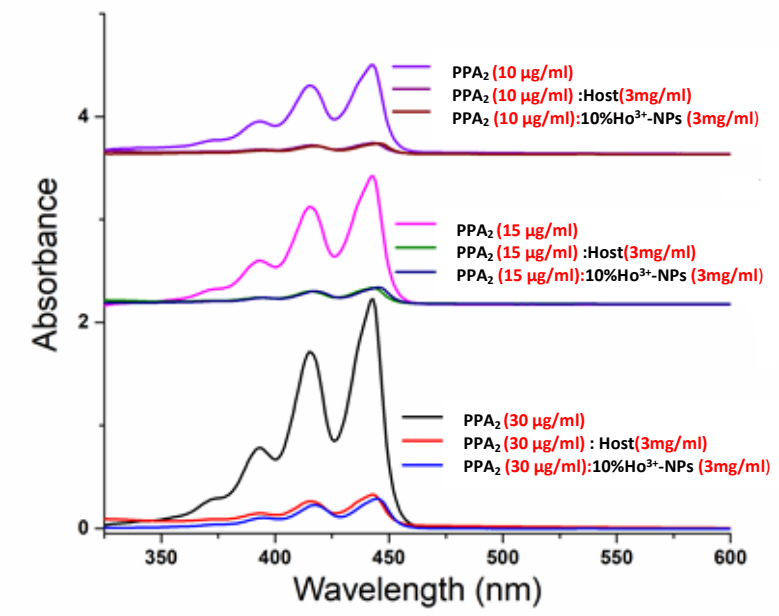

Figure 4.3: Absorption Spectra of different series 10%Ho^{3+}-NPs/PPA_2 – Dye binding based on Table 4.1

Figure 4.3 shows the absorption spectra of the samples from table 4.1. The 10%Ho^{3+}-NPs were used There are three absorption peaks at 396, 419 and 450 nm and as the Dye concentration increases the intensity of the peaks are more enhanced. Moreover, in the most concentrated Dye solution (1:100) the absorption of the light, is 3 times higher than that of the lowest Dye concentration (ratio 1:300). In all the systems (free PPA_2 solution, x%Ho^{3+}-NPs:PPA_2 solution and $NaYF_4$-NPs:PPA_2 solution), the case of weight ratio of 1:100 showed up the strongest absorbance.

After the addition of the NPs in the final solutions the intensities decrease significantly with a simultaneous blue shift of the absorption bands. Additionally, the system with inert NPs and that with active NPs have a slight difference in their absorbance intensities.

The samples that contain only free organic molecules have strongest absorption bands in comparison to those containing both inert or active NPs (inert or active). The existence of NPs plays a vital role in the quenching of the absorption bands of the solutions.

As a short summary, the Dye concentration has an important role in determining the absorbance intensity. The free Dye solutions have higher absorbance in comparison to the systems bound with NPs. The UCNPS for this study show the lowest absorption bands in comparison to other samples of the same dilution level. More absorption spectra can be found in Appendix 2.

4.3 Emission Spectra (λ_{ex}=396 and 431 nm)/Xenon Lamp

Binding System: 10%Ho^{3+}-NPs/PPA_2

The first goal of these measurements was to get an insight, in order to determine how the emission bands change as the amount of the Dye in the solution increases. The second goal was to compare the emission bands of the Dye sensitized Ho^{3+}-NPs (active system) with the Dye sensitized host NPs (inert system).

Two different excitation wavelengths, 396 and 431 nm (Fig. 4.4 and 4.5, respectively), were used with a Xenon Lamp as an excitation source. The first was the excitation wavelength only workable for Dye absorption(396nm) and the second was the excitation wavelength for both Dye and Ho^{3+} (431nm) mainly and slightly respectively. These excitation wavelengths were based on the absorption bands of Ho^{3+} and PPA_2 (Fig. 1.2). The binding systems that used for these recordings were the same as in the absorption spectra.

According to Fig. 4.4 (λ_{ex}=396 nm), as the Dye concentration increases, the intensity of the trends around 450, 485 and 515nm increases as well. This increase can be attributed only to the Dye contribution because of the increasing concentration of Dye molecules in THF solvent. When inert or active NPs were added to the final solution the emission spectra bands decrease significantly in comparison to those samples that contain only free organic molecules in THF. Moreover, the inert binding system shows higher emission levels compared to the active binding system. Also, the intensity of the active binding system is three times lower that of free Dye solution, and there is a simultaneous red shift of the bands. The same pattern is followed for all the Dye concentrations of 30, 15 and 10 μg/ml with a standard concentration of NPs (3 mg/ml). As PPA_2 concentration increases, stronger emission bands were observed. Briefly, this is an additional confirmation that the presence of Dye molecule can boost the overall intensity of the binding systems.

In Fig. 4.4b the magnification of the emission spectra for PPA_2:Ho^{3+} -NPS of in the three dilution levels is presented. The main reason for the magnification at this wavelength was to observe the impact of the Dye concentration in the red emission intensity of Ho^{3+}. The peak at 648 nm belongs to Ho^{3+} transitions and is attributed to 4f-4f transitions from $^5F_5 \rightarrow {}^5I_8$ of Ho^{3+}. This peak increases as the concentration of the Dye molecule increases in the binding system. Although excitation light ~ 396 nm was chosen to only excite the Dye molecules, the red emission peaks from Ho^{3+} at 648nm were also observed because of efficient energy transfer from PPA_2 Dye to Ho^{3+}-NPs.

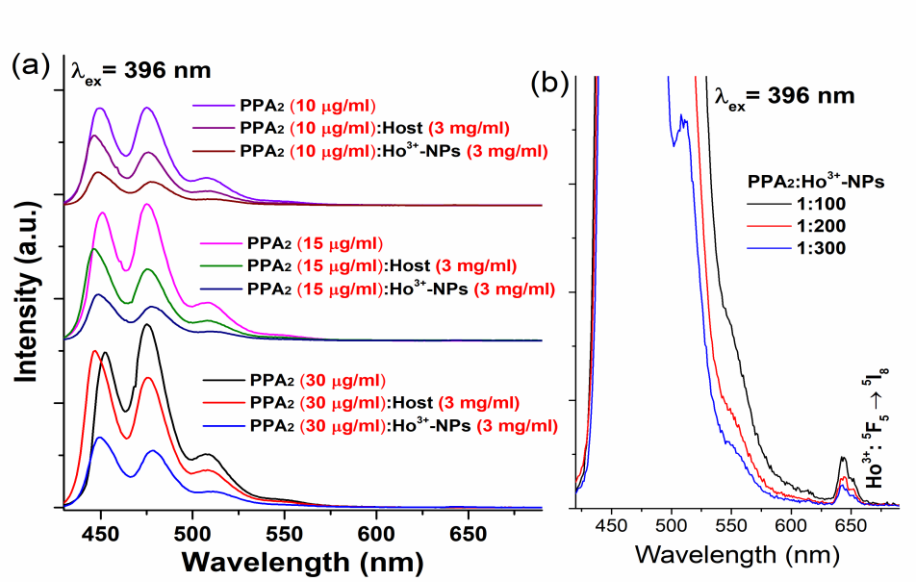

Figure 4.4: (a) Emission Spectra (λ_{ex}=396 nm) of different series 10%Ho^{3+}-NPs/PPA_2 – Dye binding system (b) Magnification at 648 nm band from Ho^{3+} emission peak.

The emission Spectra of the samples measured under excitation wavelength of 431 nm are depicted in Fig. 4.5. This wavelength was used to excite Ho^{3+} and PPA_2 at the same time (Fig. 1.2). The spectra of the samples that were recorded show many similarities with those at λ_{ex}=396nm. The main difference is that the intensity of the emission bands is stronger than in Fig. 4.5. After magnification the emission at 648 nm (Ho^{3+}:$^5F_5 \rightarrow {}^5I_8$) shows that the peak at 1:100 is three times higher that at 1:300 and double that of at 1:200 weight ratio.

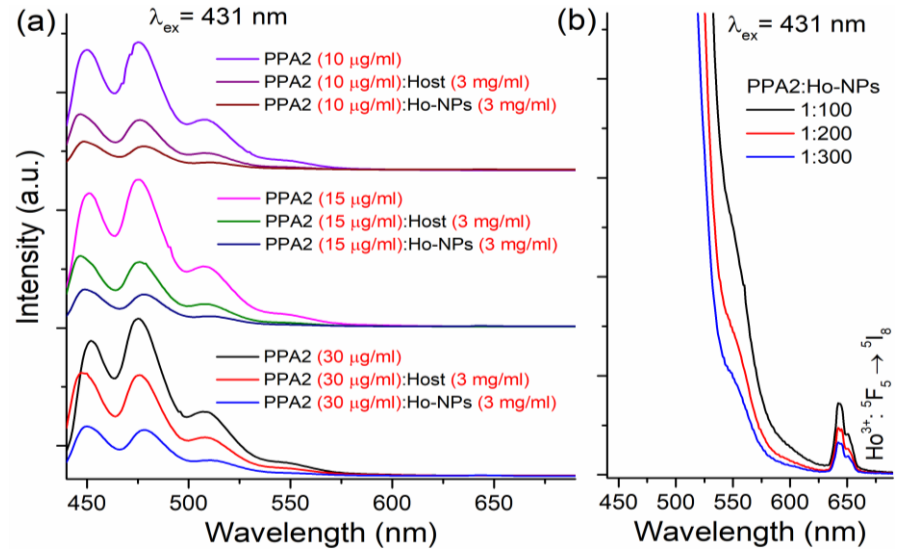

Figure 4.5: (a) Emission Spectra (λ_{ex}=431 nm) of different series 10%Ho^{3+}-NPs/PPA_2 – Dye binding system. (b) Magnification at 648 nm which is Ho^{3+} emission peak.

The results from both 4.4 and 4.5 Fig., indicate that the Dye sensitized Ho^{3+} NPs are promising for an enhanced blue-to-UV UC .More emission spectra can be found in Appendix 3.

4.4 Excitation Spectra

Binding System: x%Ho^{3+}-NPs /PPA_2

To prove that efficient energy transfer from Dye to NPs takes place, excitation spectra from different binding systems, Dye solution, and colloidal x%Ho^{3+}-NPs solution were measured by monitoring the emission wavelength at 643 nm. The samples used here are x%Ho^{3+}-NPs/PPA_2, $NaYF_4$-NPs/PPA_2, free PPA_2 and x%Ho^{3+}-NPs (ratios 1:100, 1:200, 1:300) (Fig. 4.6).

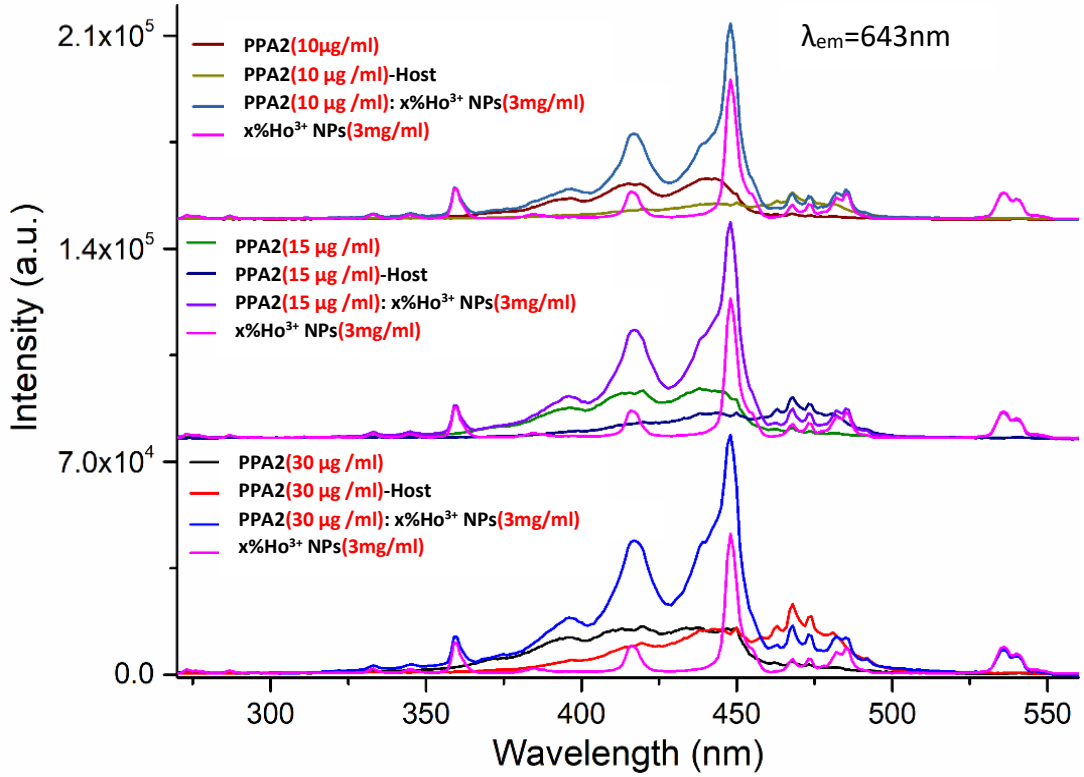

Figure 4.6: Excitation Spectra of different series x%Ho^{3+}-NPs/PPA_2– Dye binding system. (λ_{em}=643 nm).

The excitation bands of the inert binding system, $NaYF_4$-NPs/PPA_2, match with that of free PPA_2. Moreover, the excitation spectra of active binding system, x%Ho^{3+}-NPs/PPA_2, match well with that of x%Ho^{3+}-NPs solution. Three main peaks were observed at 360, 420 and 450 nm due to electronic transitions of Ho^{3+} ions. The wavelength monitored for this excitation spectra is one of the characteristic peaks of Ho^{3+} at 645 nm corresponds to the electronic transition $^5F_5 \rightarrow {}^5I_8$. The well overlapped excitation peak from Ho^{3+} ions and that from PPA_2 Dye molecules reveal the occurrence of energy transfer from Dye to Ho^{3+} ions.

4.5 Dye Sensitization

An important experimental proof about the sensitization of PPA_2-Dye to Ho^{3+}NPs is the matching of absorption spectra of PPA_2-Dye and excitation spectra monitoring UV-B UC luminescence for the active binding system (Fig. 4.7a). The aim was to measure the UV-B UC peak of the 10%Ho^{3+}NPs-PPA_2 binding system with step of 1 nm from 410 to 460 nm and then the peak intensity of every UV-B UC band was plotted as function of excitation wavelength. Noted that the output energy of OPO laser shows higher energy in the range of 410-460 nm (Fig. 4.7b). This will have direct influence on the shape of excitation band, such as a sharp peak obtained at about 417 nm (Fig. 4.7a). In general, the overlapping trends observed in Fig.4.7 reveals that the goal of this experiment was achieved and the Dye sensitization was proved.

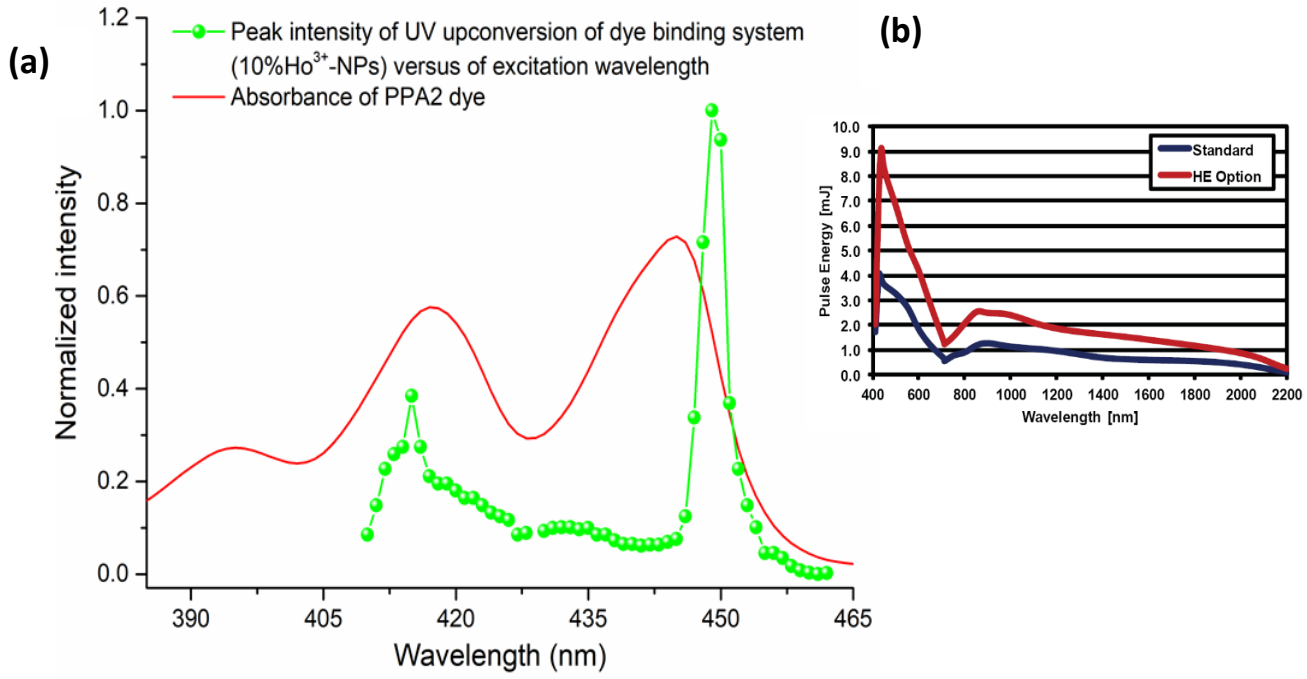

Figure 4.7: (a) Match of the excitation spectra (10%Ho^{3+}-NPs) and the absorption spectra of PPA_2-Dye, in order to prove the occurrence of the Dye sensitization. (b) In the right side of the figure there are OPOLETTE/UV Tuning Curves. The comparison of the curves proves the High pulse Energy of the OPO Laser.

more

4.6 Blue –to-UV UC Spectra/OPO Laser

Binding System: 10%Ho^{3+}-NPs/PPA_2

The following experimental part was focused on the UC spectra from blue (λ_{ex}=447 nm) to UV-B (λ_{em} =312 nm) with the use of OPO Laser as the excitation light source. The first intention of these measurements was to observe the UC peaks, to determine which concentration of the antenna enhance the UC peak ~ 310 nm and to verify which excitation wavelength gives the highest intensity UC peaks.

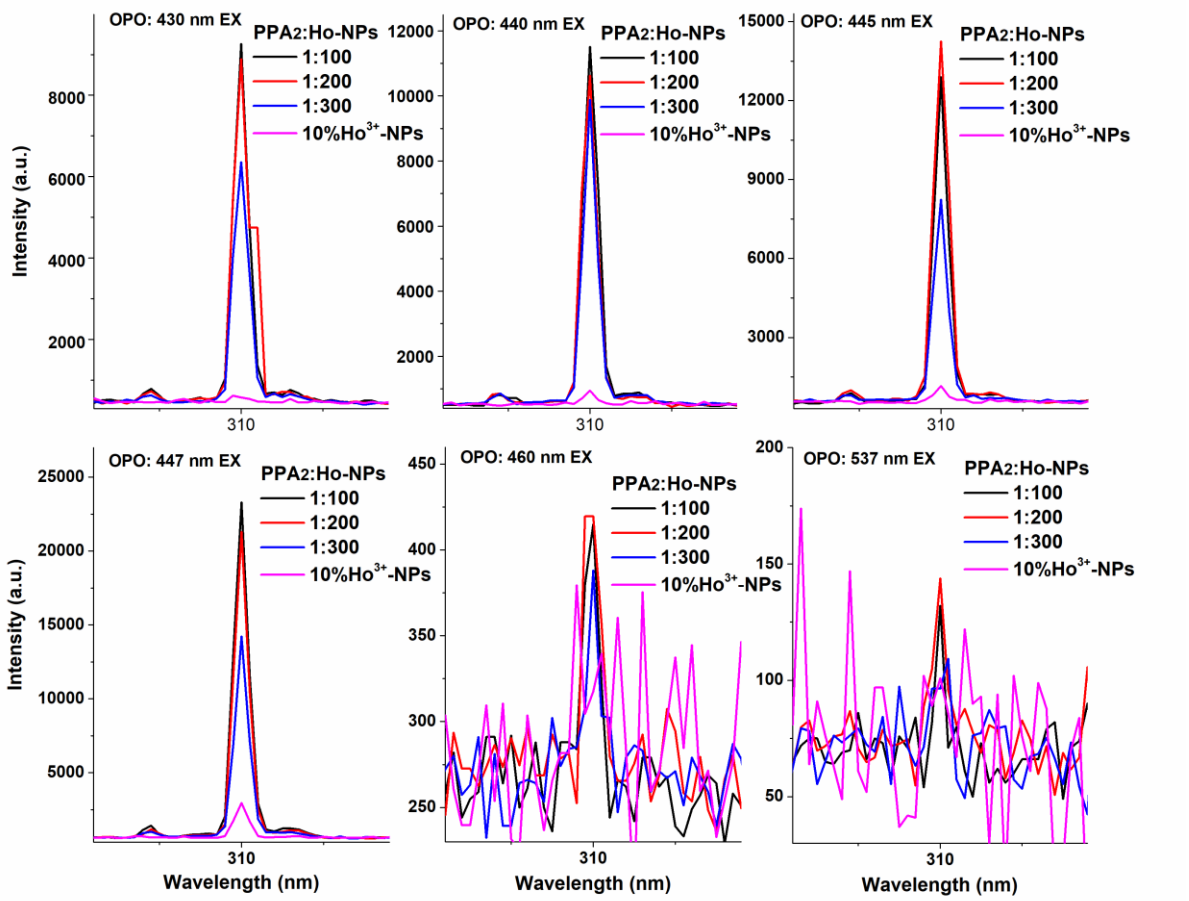

Figure 4.8: Upconversion peaks of different series 10%Ho^{3+}-NPs/PPA_2 – Dye binding system. The samples excited at 430, 440, 445, 447, 460 and 537 nm

The samples that were recorded for their UC properties were PPA_2:10%Ho^{3+}-NPs (1:100, 1:200 and 1:300) and 10%Ho^{3+} NPs. Based on the absorption spectra Fig.4.3 and the excitation spectra Fig 4.6 the excitation wavelengths employed here were 430, 440, 445, 447, 460 and 537 nm, respectively. In each excitation wavelength the intensity of UC peaks were recorded and compared.

The peak recorded at 310 nm in Fig. 4.8 belongs to the emission of Gd^{3+} ion and specifically to the electronic transition from ^6P_j-> $^8S_{7/2}$. Here an efficient two-blue photons-involved ETU process is proposed for the intense UV-B UC luminescence. Within the hybrid upconverting nanomaterials, energy transfer occurs from Dye →2 (individual) photon* (Ho^{3+}) energies→ 1 photon* Gd^{3+} energy with high efficiency as described in Chapter 2. In order to prove this mechanism more experiments are needed.

Among the four samples whose UC properties were recorded, the case of 10%Ho^{3+}-NPs:PPA_2 (~ 1:100) and 10%Ho^{3+}-NPs samples pointed out the highest and the lowest UC peak, respectively. At λ_{ex} =447 nm (both Dye and Ho^{3+} contribute to the UC process), the sample of PPA_2 Dye -Ho^{3+}-NPs(~ 1:100) shows 10 times stronger UC intensity at 310nm in comparison to bare NPs. That confirms the successful function of the antenna to enhance the UC intensity. At λ_{ex}=430 nm Ho^{3+} was not excited, but at the 1:100 weight ratio the UC peak intensity was still much intense, around 9000 a.u. In contract to that when the samples are excited at 447 nm (both Dye and Ho^{3+} were excited), the highest UC peak has intensity 24,000 a.u., almost 3 times that of 430 nm. From the absorption spectrum of Ho^{3+}, it is known that the absorption at 430 nm is at least hundreds of times weaker than that at 447 nm(section 1.3). This directly suggest that the sensitization of Dye to Ho^{3+} takes place rather efficiently after binding as hybrid system.

Based on the UC results of Fig. 4.8 the UC intensity peaks at 447 nm showed the best results in comparison to other excitation wavelengths. It was also proved that ETU mechanism works due to the fact that UC peaks are observable even without Dye attached on the surface of Ho^{3+} NPs. The aim to attach PPA_2 on the surface of the NPs and record enhanced UC peak intensity was achieved and proved. More UC spectra of different binding systems with different Ho^{3+} concentrations were studied and depicted in Appendix 4.

Binding system: X%Ho^{3+}-NPs/ With and Without PPA_2

The UC peaks that were recorded in Fig. 4.8 were for 10%Ho^{3+}-NPs:PPA_2(1:100). The next goal was to determine which Ho^{3+} concentration contributes to higher intensity UC peak. UC peaks were recorded from NPs which were synthesized in various Ho^{3+} concentrations (Fig. 4.9). To understand in-depth the influence of the dopant the samples were excited at 447 nm. The UC peaks in Fig. 4.9 showed that 8%Ho^{3+} can give strongest UC peaks in comparison to 12% Ho^{3+}. Noted that 8% and 1% Ho^{3+} show almost the same UC intensity. This is not consistent and may come from error in the measurements.

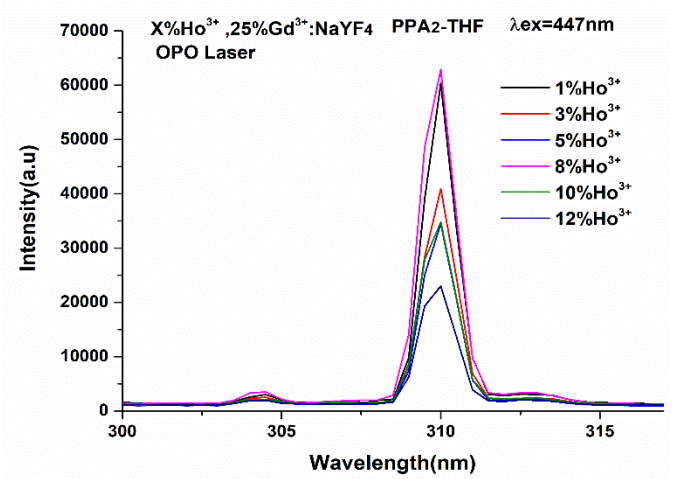

Figure 4.9: Upconversion peaks for different concentrations of x%Ho^{3+}-NPs/PPA_2 – Dye binding, excited at 447nm.

Another aim was to prove that the same NPs without Dye attached on their surface indicating lower UC peak intensity (fig. 4.10). NPs 1%Ho^{3+} without Dye attached on their surface proved the strongest UV-B UC. The intensity of the UC peak when Dye is present is 7 times higher than this when it is absent. Subsequently, it was proved that the Dye attachment gives impressive difference in the UC peaks.

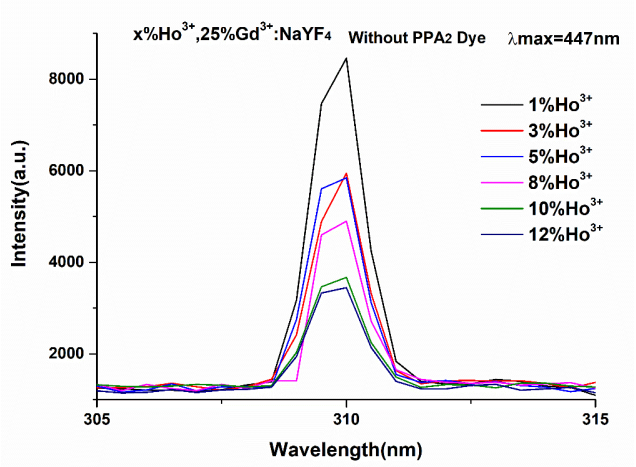

Figure 4.10: Upconversion peaks for different concentrations of x%Ho^{3+}-NPs without Dye excited at 447nm.

4.7 Blue –to-UV UC Spectra/Xenon Lamp

Binding System: 10%Ho^{3+}-NPs/PPA_2

OPO Laser was used until now to verify the UC event in blue-to-UVB UC because of its high pulse energy. In the following experiments presented, Xenon Lamp was used instead of the OPO Laser as an alternative blue light source in an effort to check if UC peaks are still observable when using a light irradiation with lower power density.

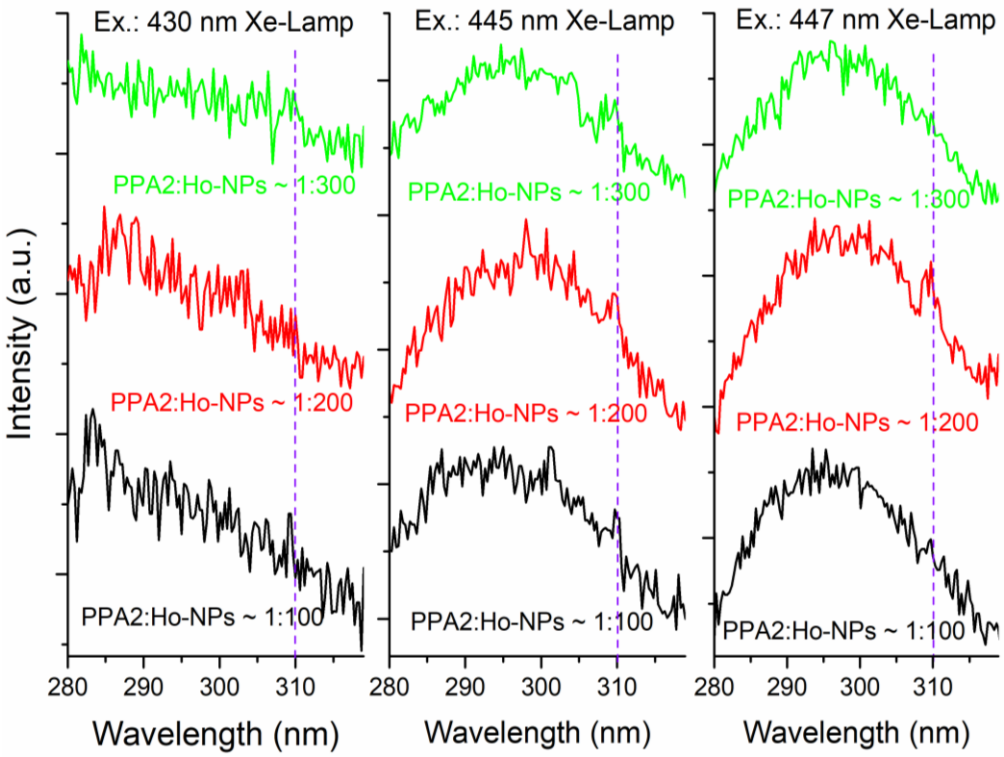

Figure 4.11: Upconversion peaks of different series 10%Ho^{3+}-NPs/PPA_2 – Dye binding system using Xenon Lamp. According to Table 2. Excited at 430, 445 and 447 nm

The samples with the Dye sensitized NPs were excited at three different wavelengths and the emission was recorded at 310 nm, which is the desired wavelength for skin psoriasis. The weight ratios of the samples were 1:100 (black lines), 1:200 (red lines) and 1:300 (green lines) (Fig. 4.11). The samples excited at 430, 445 and 447 nm are depicted horizontally. At 447 nm a small curve around 310 nm was formed in comparison to 430 and 445 nm but still cannot considered as real UC peak.

Examining the graphic curves vertically, the samples with different weight ratios but with excitation at the same wavelength are presented. Only at 447 nm small curves appeared but these cannot be also considered as UC peaks. Specifically, the curve representing the 1:100 weight ratio is 3 times strongest than that representing the 1:300. That was expected because the 1:100 weight ratio contains 3 times higher Dye concentration in comparison to 1:300. It can be concluded that Xenon lamp is not strong enough to get any UC peak even in a binding system.

4.8 Blue-to-UV UC Spectra /CW Laser

Binding System: 10%Ho^{3+}-NPs/PPA_2

The OPO laser that was used for detecting the UC peaks, is a pulsed Laser. In order to check if these peaks can be also observed with a continuous wave laser, the CW Laser was also used for measurements where samples were excited at 447nm and recorded from 280nm to 360nm.

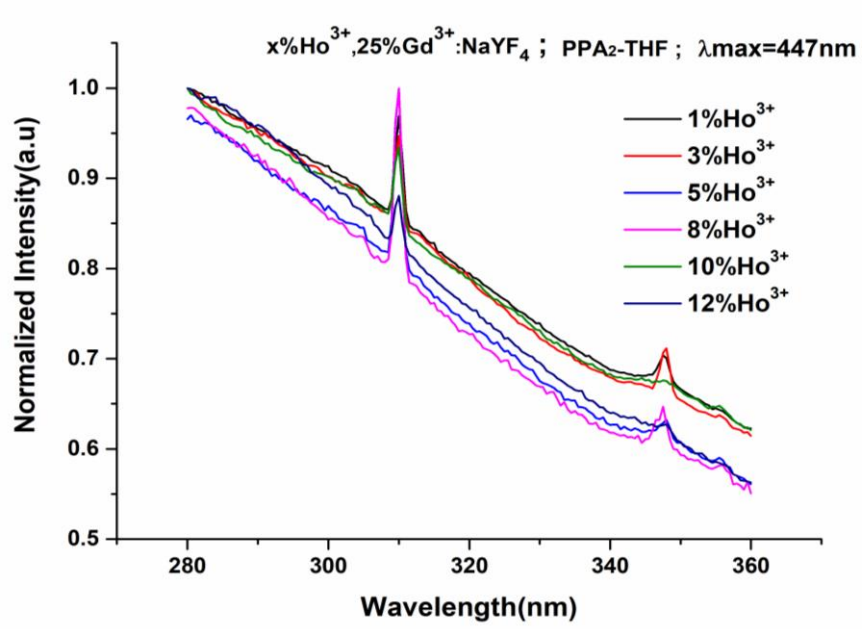

Figure 4.12: Upconversion peaks for different concentrations of x%Ho^{3+}-NPs/PPA_2– Dye binding system, excited at 447nm using CW Laser, excited at 447 nm. With Optical filter that absorbs the UV photons from CW laser

It is obvious from Fig. 4.12 that peaks are observed at 310 nm and at 345nm. The peak at 310 nm indicates the energy transfer from two Ho^{3+} (added up energy) to one Gd^{3+} and is the UV-B UC peak that we are mainly interested in. It should be mentioned that although in the previous experiments the intensity of UC peaks changes by varying the Ho^{3+} concentration, now the observed UV-B UC peak doesn't change as a function of the Ho^{3+} concentration. This can be explained by the intense background likely from light reflection in the measurements. The peaks at 345 nm can be assigned to the $^5G_3 \rightarrow {}^5I_8$ electronic transition of Ho^{3+} ions.

4.9 Decay Curves

Decay curves can provide information about the excited state lifetime, the radiative and non-radiative decay processes and the energy transfer rates. The first intention of these measurements was to optimize the difference in decay curves after attaching the organic molecules on the surface of Ho^{3+}-NPs. Following this, the next idea was to prove that there is efficient energy transfer from PPA_2 to Ho^{3+} ions in the host lattice, likely with FRET mechanism (Chapter 2)

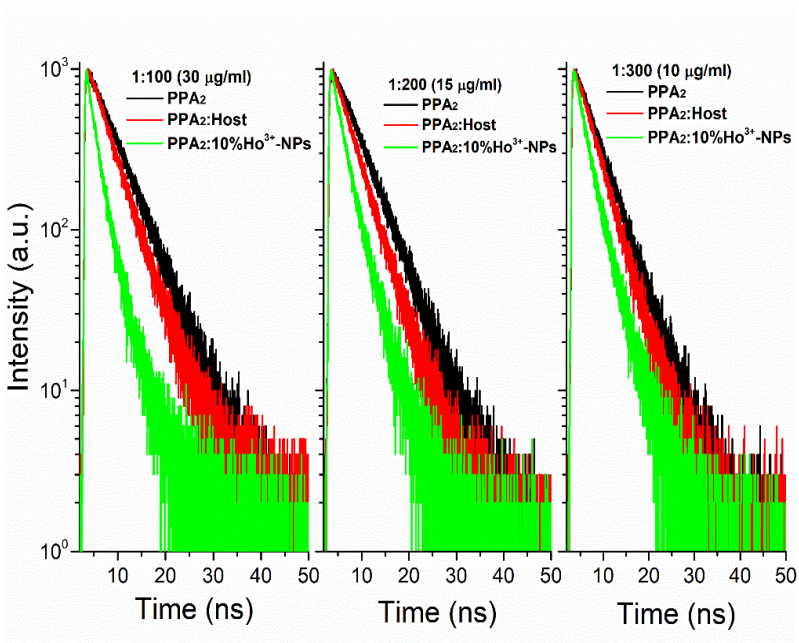

Figure 4.13: Lifetime measurements of different series 10%Ho^{3+}-NPs/PPA_2 – Dye binding system (Table 2). Excited and Emitted at 405 and 500 nm respectively.

The experiments that were conducted proved that the solution with the free Dye has longest lifetime compared to the other samples as illustrated in Fig. 4.13. The fastest decay was recorded for the solution containing 10%Ho^{3+}-NPs/PPA_2. and the slowest for the solution that contains only free Dye molecules-dissolved THF. To compare with the lifetime of $NaYF_4$-NPs/PPA_2 inert binding system, the obviously shorter lifetime of the 10%Ho^{3+}-NPs/PPA2 active binding system reveal the efficient energy transfer happened from PPA_2 Dye to Ho^{3+} ions. Moreover, the 1:200 and 1:300 solutions followed the same pattern as the 1:100. Although the different dilution levels follow the same pattern the solution with the highest PPA_2 concentration (1:100) showed the most obvious difference in the decay times of the samples.

In the light of more valid conclusions more lifetime recordings were performed. Specifically, lifetime measurements were performed in solutions with fixed ratio 1:100 (most promising) and NPs doped with various Ho^{3+} concentrations. In Fig. 4.14 the decay curves of six samples are depicted. Additional, Decay Curves can be found in Appendix 5.

Binding Systems: X%Ho^{3+}-NPs /PPA_2

Lifetime measurements were performed for x%Ho^{3+}-NPs/PPA_2 (x=1,3,5,8,10,12 %) at binding case of mass ratio ~ 1:100. The purpose of the recordings at 500 nm was to check the efficiency of the energy transfer from PPA_2 Dye to NPs.

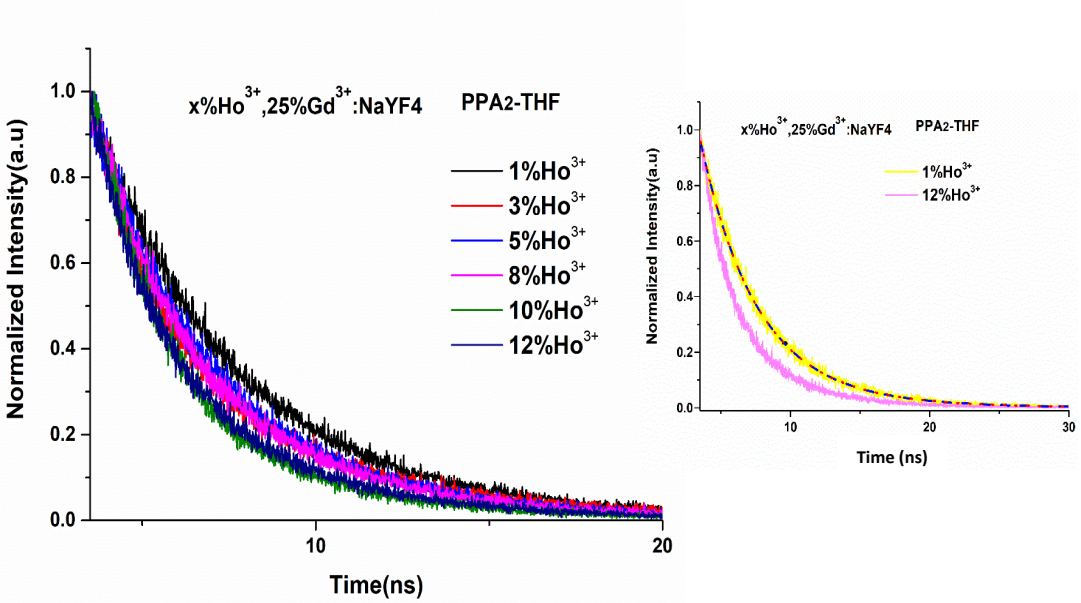

Figure 4.14: Lifetime measurements for X%Ho^{3+} NPs (x=1, 3, 5, 8, 10, 12). Excited and Emitted at 405 and 500 nm respectively.

In Fig. 4.14 a decrease in the lifetime for the Dye sensitized co-doped NPs is observed as the amount of Ho^{3+} dopants increase. This indicates that the concentration of Ho^{3+} has an important role in the energy transfer process. Specifically, as the Ho^{3+} concentration increases, more Ho^{3+} ions absorb energy and subsequently more energy is transferred from the Dye to the Ho^{3+}-NPs. The difference in lifetime between the lowest and the highest Ho^{3+} samples is depicted in Fig. 4.14. Consequently, the more Ho^{3+} present the shorten of the decay time.

Binding Systems: X%Ho^{3+}-NPs /PPA_2

From Dieke diagram it is known that the energy gap between the ground state and the first excited state of Gd^{3+} is very large and hence its luminescence cannot be easily quenched by phonon relaxation, having a relative long lifetime. The aim of these measurements was to verify if there is back energy transfer from the first excited state of Gd^{3+} to the UV-excited state of Ho^{3+} (1:100 weight ratio).

Using the same binding systems as above-mentioned, OPO Laser was now used as a light source (λ_{ex}=447 nm, λ_{em}=310 nm) to record their lifetime (Fig. 4.15). The emission wavelength at 310 nm is purely associated with the Gd^{3+} ion and its emission from the ^6P_j to $^8S_{7/2}$ state.

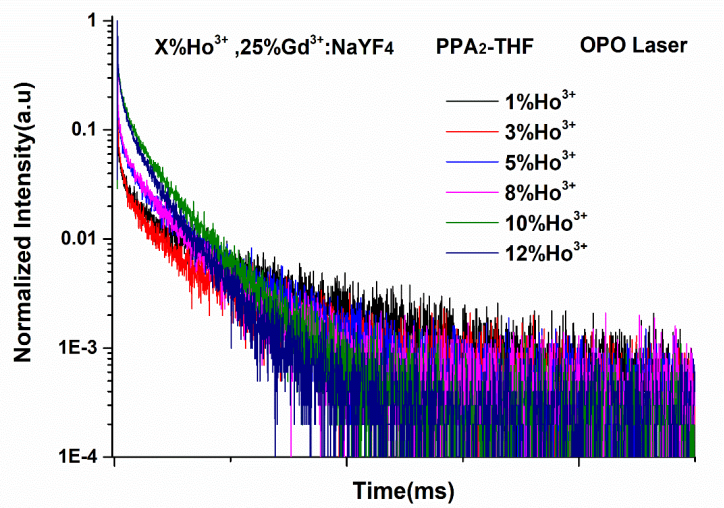

Figure 4.15: Lifetime measurements for X%Ho^{3+}- NPs/PPA_2. Excitation and emission wavelengths 447 and 310 nm respectively.

Under UC conditions it was showed that the concentration of 12%Ho^{3+} has the shortest lifetime, as presented in Fig. 4.15. That means that the more we increase the concentration of Ho^{3+} dopants the faster is the decay time. This observation implies the occurrence of back energy transfer from the first excited state of Gd^{3+} (^6P_j) to the UV-excited state of Ho^{3+} ($^3M_{10}$). That is a strong proof that a high increase of the dopant concentration can lead to non-desired processes.

4.10 Ligand Exchange with $NOBF_4$

Ligand Exchange with $NOBF_4$ in DMF is another binding method which was described in Chapter 3. According to this method the CC- Dye will be bound strongly on the surface of the NPs relative to the direct mixing method. The aim of these experiments was to examine a different binding method and get information about the function of a different antenna. Spectroscopic measurements such as absorption. and UC measurements were performed. The binding systems and the comparisons among the systems are still the same as in the direct mixing procedure.

Binding System: 10%Ho^{3+}-NPs /CC-Dye

Absorption Spectra

The absorption Spectra were recorded for CC-Dye: Host NPs and for CC-Dye :Ho^{3+} ,Gd^{3+}NPs. In these experiments the concentration of the Dye bulk was 10 times higher in comparison to Dye bulk solution of the direct mixing bulk solution. The reason was simply to test the influence in the values of the spectroscopic measurements with more concentrated Dye bulk solution. The NPs concentration was 3 μg/ml and the initial CC-Dye solution was 0.1 mg/ml.

Figure 4.16 represents binding systems with Dye sensitized host NPs and Dye sensitized co-doped NPs. The absorption bands of the samples increase as the concentration of the CC-Dye increases in the final solution.

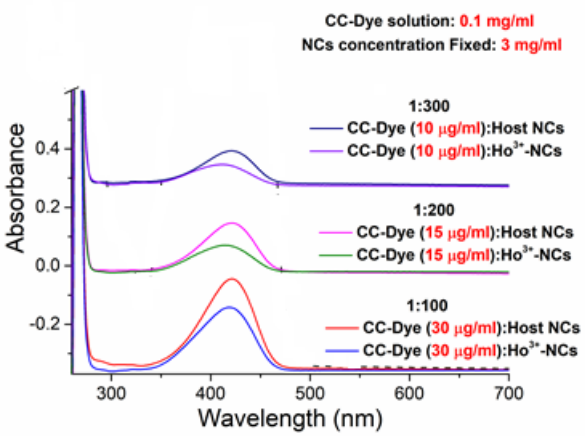

Figure 4.16: Absorption Spectra of different series 10%Ho^{3+}-NPs/CC– Dye binding System.

This can be explained because more Dye molecules in the solution absorb more light. Moreover, the CC- Dye host NPs still show stronger absorption bands in comparison to CC-Dye co-doped NPs. These results are compatible with the absorption Spectra of the Direct Mixing Method. and weight ratio 1:100 still shows the best results. Briefly, the concentration of the Dye molecule has a big impact on the absorption intensity of both samples.

Blue –to-UV UC Spectra/OPO Laser

In the next experiments a CC-Dye molecule was attached on the surface of the NPs and the Blue to UVB UC peaks from Gd^{3+} at 310 nm was recorded. OPO Laser was used again as an excitation light source. The weight ratios and the concentration of NPs remained the same as previously. In Fig. 4.17 it is presented that all weight ratios have peak at 310 nm but 1:200 shows the highest UC peak at 310 nm, which is the outcome of the unique emission of the Gd^{3+}. Based on previous UC results it was expected to observe the highest UC peak for 30 µg/ml CC-Dye (1:100) and not at 15 µg/ml.

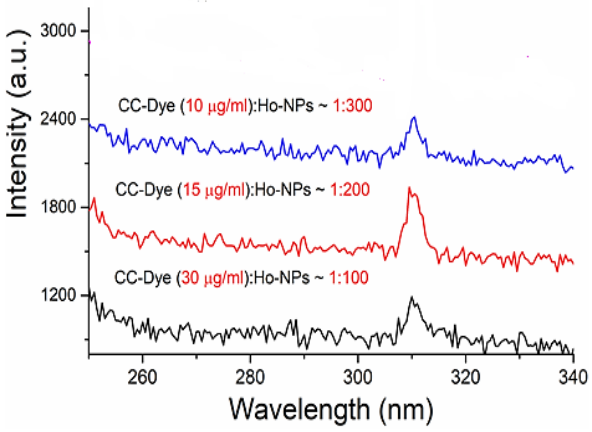

Figure 4.17: Upconversion peaks of different series 10%Ho^{3+}-NPs/CC– Dye binding system. The samples excited at 430 nm. OPO laser was the excitation source.

This can be attributed to an unsuccessful binding process during the experimental steps. In general, UC peaks at 310 nm were observed for ligand exchange with $NOBF_4$ although they were not so strong as the UC peaks recorded from the direct mixing binding method.

Conclusions and Outlook

Direct Mixing

Spectroscopic measurements of three different samples (PPA_2, PPA_2: host-NPs, PPA_2:Ho^{3+}-NPs) in different weight ratios NPs:Dye (1:100, 1:200, 1:300) were conducted. Moreover, Förster Resonance Energy Transfer (FRET) sensitization scheme, to overcome the weak absorption of intra-4f transitions of Ho^{3+} ion, was successfully achieved by the systematic exploration of respectively binding two kinds of designed organic Dye molecules with the UV-B upconverting nanoparticles.

The absorption spectra indicate that PPA_2 Dye with intense broadband absorption around 450 nm will favor the sensitization effects. It was also proved that as the concentration of PPA_2-Dye increased in the final solution the absorption of the UCNPs increased as well, revealing that the amount of the Dye in the final solution has an impact in the absorption of the light.

Dye sensitization was also achieved with the perfect match of the absorption Spectra of Dye molecules with the Excitation Spectra of PPA_2:10%Ho^{3+} -NPs. The last was created by monitoring the UC peak in each wavelength.

Dye-sensitized Blue-to-UVB UC was successfully achieved for the PPA_2:10%Ho^{3+} -NPs hybrid binding system. Strong UC peaks at 310 nm were recorded under excitation of Dye molecules using an OPO Laser. At the same time it was also proved that the more Dye molecules in the final solution the stronger the UC luminescence from Gd^{3+} ($^6P_j \rightarrow {}^8S_{7/2}$).

Decay Curves (λ_{ex}=400 nm and λ_{em}= 500 nm) showed a decrease in the lifetime of the PPA_2 Dye as the NPs were added in the final solution and proved that efficient energy transfer from the Dye to the NPs. Furthermore, lifetime measurements under UC conditions (λ_{ex} =447 nm and λ_{em}= 310 nm) proved the presence of back energy transfer from the excited state of Gd^{3+} to the UV-excited state of Ho^{3+}. Subsequently the amount of the sensitizer can enhance the back energy transfer process.

Ligand Exchange with $NOBF_4$

Blue-to-UVB UC was also achieved using ligand exchange with $NOBF_4$ to bind the CC-Dye on the surface of NPs. However, the intensities of these UC peaks were much weaker in comparison to the hybrid system made by direct mixing approach. It was also proved that the absorption intensity increases proportionally to the concentration of the antenna.

In both binding approaches, it was not successful to get UC peaks at 310 nm using Xenon Lamp as excitation light source. This can be attributed to a lower absorption/sensitization even with assistance of Dye molecules.

Outlook

The aim of this study (Dye-sensitized Blue to UVB UC) was successfully achieved. The obtained $NaYF_4$:x%Ho^{3+},25%Gd^{3+} nanophosphors can absorb blue photons around 450 nm by Ho^{3+} ions and then emit narrowband UV-B photons around 310 nm (Gd^{3+}), with energy transfer from UV-excited states of Ho^{3+} to nearby Gd^{3+} ions. However, there are still some additional experiments that could be done in order to have a better insight view of the Dye sensitization. An idea is to design and use new dye with a shorter distance between Dye-Ho^{3+}.Further optimization should be done by finding novel hosts having lower phonon energy and at same time allowing for a higher Ho^{3+}-doping content before occurrence of obvious concentration quenching. Besides, the mass ratios in the hybrid nanomaterials require further exploration in the mass ratio in order to achieve much stronger dye absorption and meanwhile achieve much more efficient sensitization effects under a tunable blue light excitation.

Appendices

Appendix 1 is the Dieke-Diagram. The other Appendices will provide information about the additional experiments which were conducted. Absorption and emission spectra for 5% NPs/PPA_2 are depicted in Appendix 2 and 3 respectively. Finally, UC spectra and Decay Curves for 5% and 12%Ho^{3+} NPs/$PPA_2$are depicted in Appendices 4 and 5 respectively.

Appendix 1: Dieke Diagram

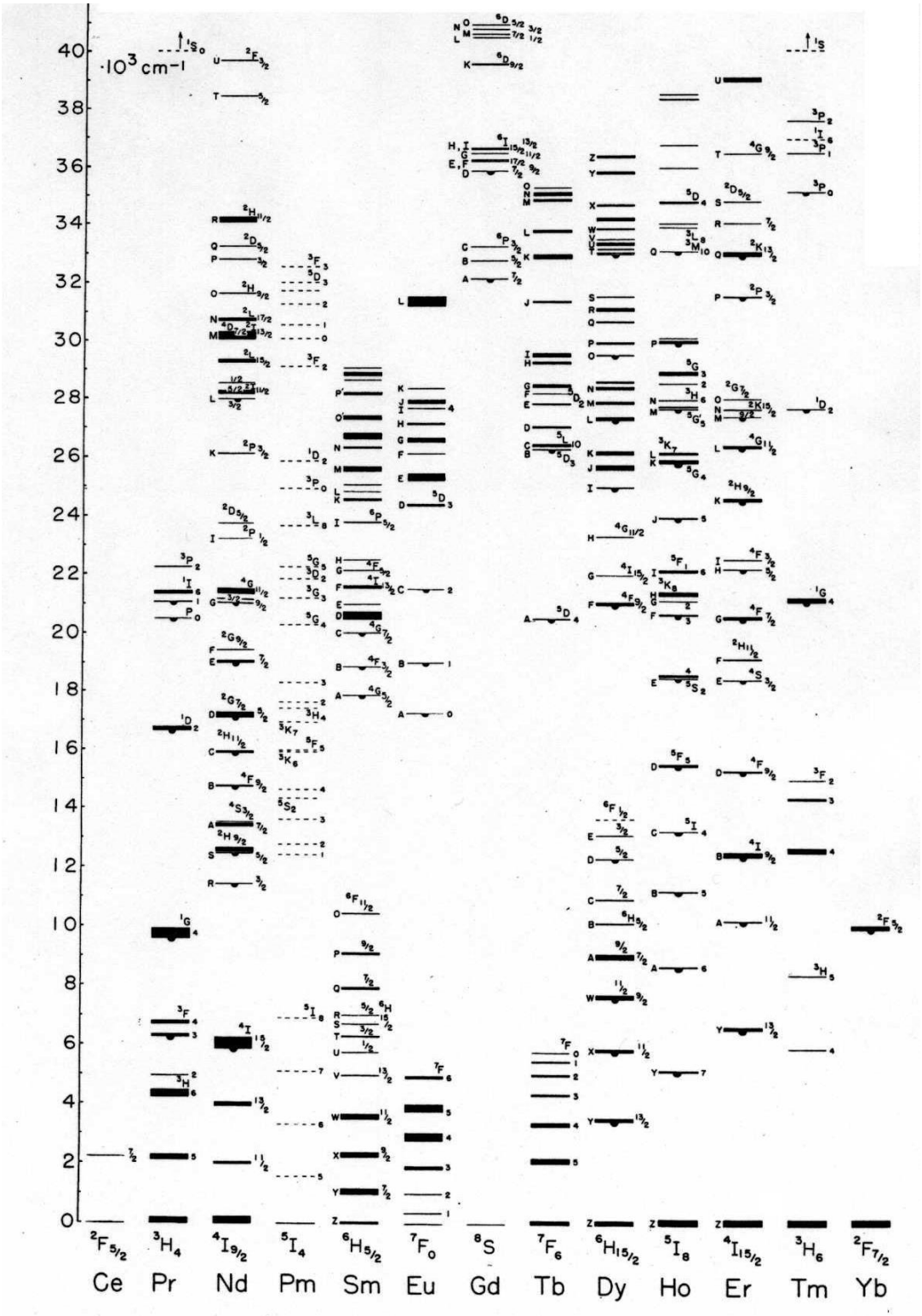

Appendix 2: Absorption spectra

Binding System: 5%Ho^{3+}-NPs /PPA_2

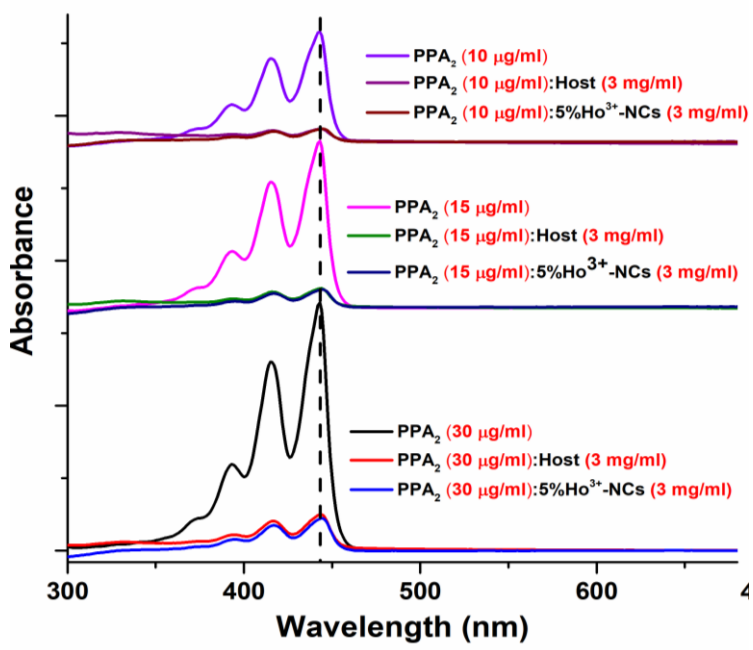

Figure 1: Absorption Spectra of different series 5%Ho^{3+}-NPs/PPA_2– Dye binding system.

Appendix 3: Emission Spectra

Binding System: 5%Ho^{3+}-NPs/PPA_2

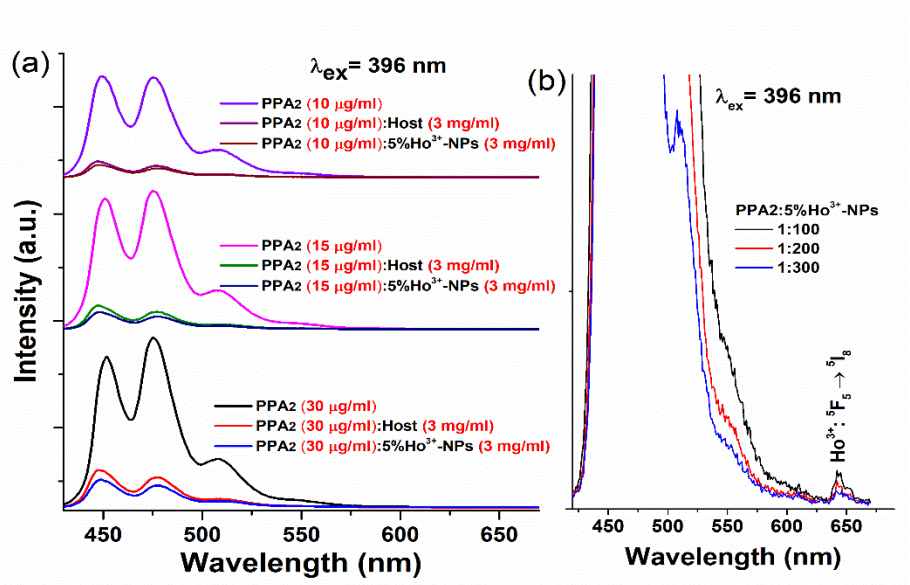

Figure 2: (a) Emission Spectra (λ_{ex}=396 nm) of different series 5%Ho^{3+}-NPs/PPA_2 – Dye binding system. (b) Magnification at 648 nm which is Ho^{3+}emission peak.

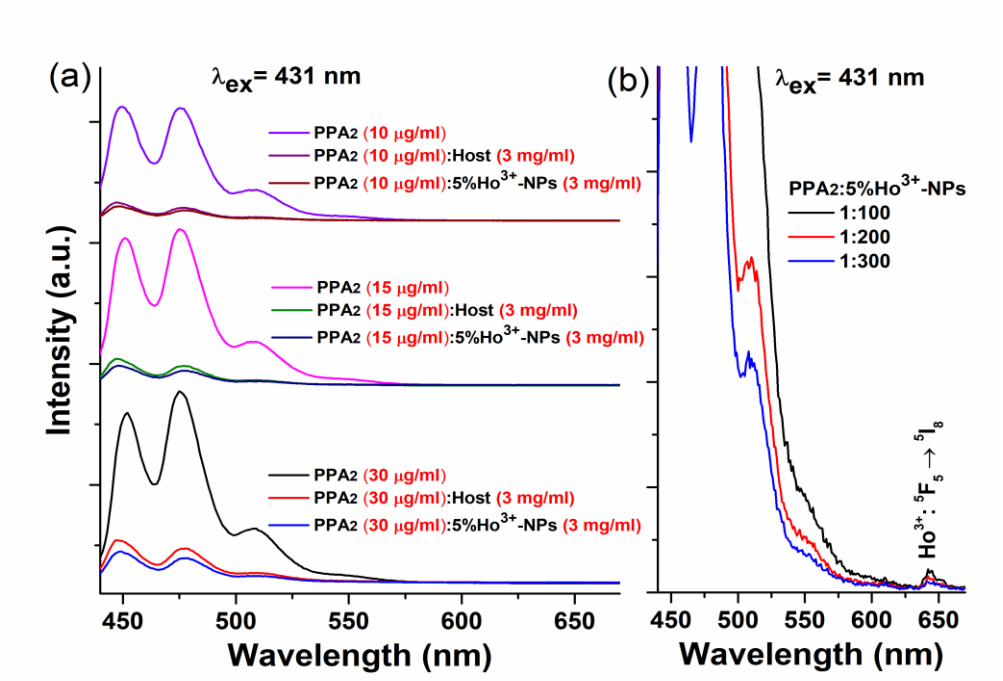

Figure 3: (a) Emission Spectra (λ_{ex}=431 nm) of different series 5%Ho^{3+}-NPs/PPA_2 – Dye binding system(b) Magnification at 648 nm which is Ho^{3+} emission peak.

Appendix 4: Upconversion Spectra

Binding System: 12%Ho^{3+}-NPs/PPA2

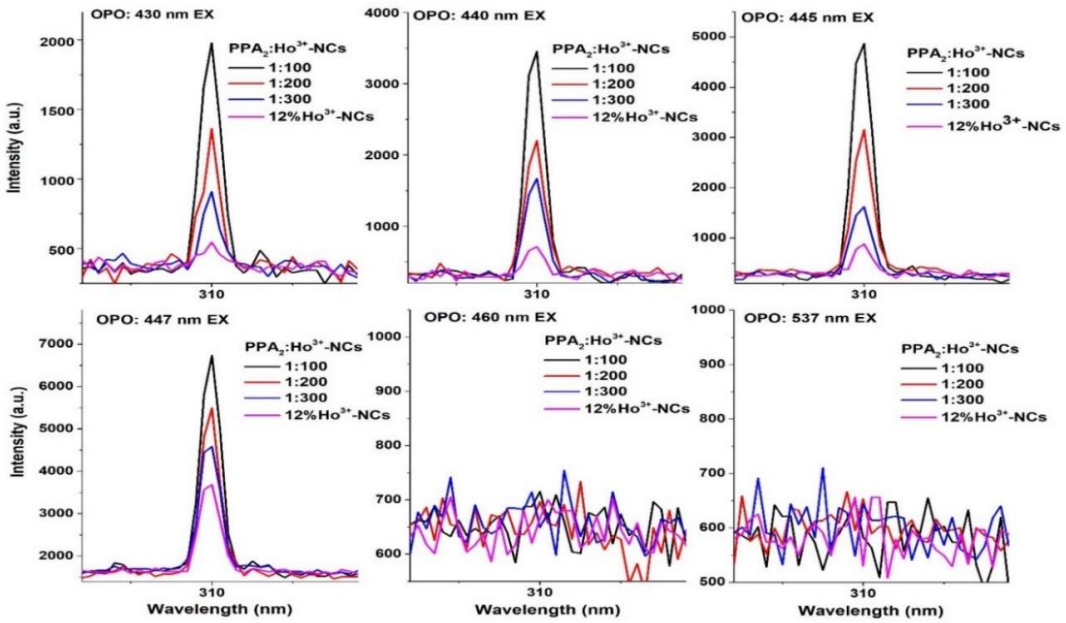

Figure 4.: Upconversion peaks of different series 12%Ho^{3+}-NPs/PPA_2 – Dye binding system. The samples excited at 430, 440, 445, 447, 460 and 537 nm.

Binding System: 5%Ho^{3+}-NPs/PPA_2

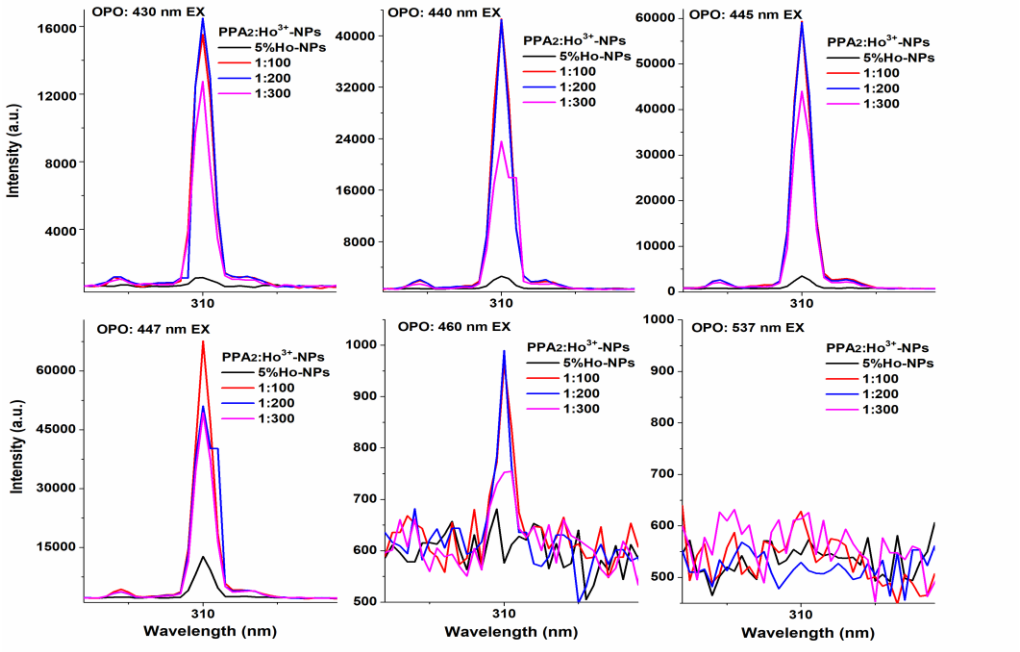

Figure 5: Upconversion peaks of different series 5%Ho^{3+}-NPs/PPA_2 – Dye binding system. The samples excited at 430, 440, 445, 447, 460 and 537 nm.

Appendix 5: Decay Curves

Binding System: 12%Ho^{3+}-NPs /PPA_2

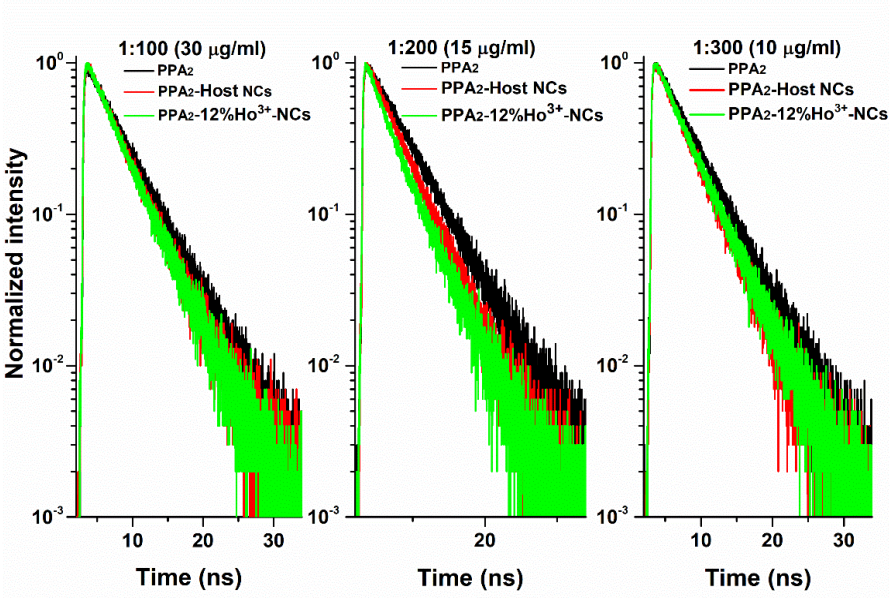

Figure 6: Lifetime measurements of different series 12%Ho^{3+}-NPs/PPA_2 – Dye binding system. Excited and Emitted at 405 and 500 nm respectively.

Binding System: 5%Ho^{3+}-NPs /PPA_2

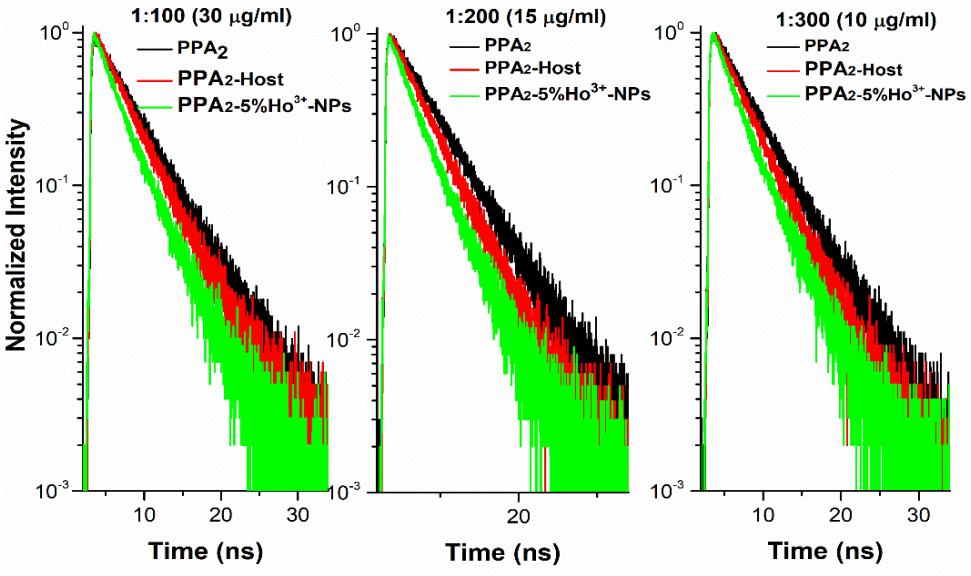

Figure 7: Lifetime measurements of different series 5%Ho^{3+}-NPs/PPA_2 – Dye binding system. Excited and Emitted at 405 and 500 nm respectively.

Acknowledgements

In this part of the thesis I would like to express my gratitude to everyone who was involved from the beginning till the end in this project. First of all, I would like to thank Professor Andries Meijerink because he gave me the chance to work in such a friendly and helpful group as condensed Matter and Interfaces. He managed to enlighten dark paths in my mind related to Spectroscopy. Moreover, I would like to thank my daily supervisor Dechao Yu for this really helpful contribution in theoretical and experimental basis. For his positive attitude that as a team we can achieve to get good and bad results. The first phrase he used to encourage me was ''results bad or good always help you to understand how something works''.

Finally, I would like to thank all CMI people, for being helpful for any kind of problem or question. More specifically II would like to thank Maike for her help with the vacuum pump. Moreover, I would like to thank Federico, Maryam, Thomas, Ryan, Philip, Tomas, Arend, Liudmyla and Nicolette for the discussions we had. Lat but not least I would like to thank all students from the master room for their friendly behavior and for the discussions we had about many issues.

References

[1] M. Tina Bhutani, MD1 and Wilson Liao, "A Practical Approach to Home UVB Phototherapy for the Treatment of Generalized Psoriasis," *Pr. Dermatol*, vol. 7, no. (2), pp. 7(2): 31–35.

[2] P. L. K. Stockbeck, E. Holze, MD, "Narrow-Band UVB(311nm) versus conventional broadband UVB with and without dithranol in photherapy for psoriasis," vol. 28, pp. 227–31, 1993.

[3] T. Gambichler, F. Breuckmann, S. Boms, P. Altmeyer, and A. Kreuter, "Narrowband UVB phototherapy in skin conditions beyond psoriasis," *J. Am. Acad. Dermatol.*, vol. 52, no. 4, pp. 660–670, 2005.

[4] F. Wang and X. Liu, "Recent advances in the chemistry of lanthanide-doped upconversion nanocrystals," *Chem. Soc. Rev.*, vol. 38, no. 4, pp. 976–989, 2009.

[5] A. M. et al. Rosa Martín-Rodríguez, Stefan Fischer, Aruna Ivaturi, "Highly Efficient IR to NIR Upconversion in Gd2O2S: Er3+ for Photovoltaic Applications," *Chem. Mater.*, vol. 25, no. 9, pp. 1912–1921, 2013.

[6] W. Zou, C. Visser, J. A. Maduro, M. S. Pshenichnikov, and J. C. Hummelen, "Broadband dye-sensitized upconversion of near-infrared light," *Nat. Photonics*, vol. 6, no. 8, pp. 560–564, 2012.

[7] J. Xu *et al.*, "Highly Emissive Dye-Sensitized Upconversion Nanostructure for Dual-Photosensitizer Photodynamic Therapy and Bioimaging," *ACS Nano*, vol. 11, no. 4, pp. 4133–4144, 2017.

[8] J. A. Parrish and K. F. Jaenicke, "Action spectrum for phototherapy of psoriasis," *J. Invest. Dermatol.*, vol. 76, no. 5, pp. 359–362, 1981.

[9] J. B. Grossweiner, "Phototherapy of Skin Disease: Science and Technology," *Sci. Phototherapy An Introd.*, pp. 299–327, 2005.

[10] J. B. Grossweiner, "CHAPTER 12 PHOTOTHERAPY OF SKIN DISEASE: SCIENCE AND TECHNOLOGY."

[11] C.-H. Y. Hao Dong, Ling-Dong, "Energy transfer in lanthanide upconversion studies for extended optical applications," *chem Soc Rev*, vol. 44, p. 1608, 2015.

[12] X. Wu *et al.*, "Dye-sensitized core/active shell upconversion nanoparticles for optogenetics and bioimaging applications," *ACS Nano*, vol. 10, no. 1, pp. 1060–1066, 2016.

[13] D. Chen, L. Liu, P. Huang, M. Ding, J. Zhong, and Z. Ji, "Nd^{3+}-sensitized Ho^{3+} single-band red upconversion luminescence in core-shell nanoarchitecture," *J. Phys. Chem. Lett.*, vol. 6, no. 14, pp. 2833–2840, 2015.

[14] G. Chen *et al.*, "Energy-Cascaded Upconversion in an Organic Dye-Sensitized Core/Shell Fluoride Nanocrystal," *Nano Lett.*, vol. 15, no. 11, pp. 7400–7407, 2015.

[15] A. Yin, Y. Zhang, L. Sun, and C. Yan, "Colloidal synthesis and blue based multicolor upconversion emissions of size and composition controlled monodisperse hexagonal NaYF4:Yb,Tm nanocrystals," *Nanoscale*, vol. 2, no. 6, pp. 953–959, 2010.

[16] K. M.-P. O. logoa and M. L. T. O. logo* Victor Gray ORCID logoa, Pan Xia ORCID logob, Zhiyuan Huang c, Emily Moses c, Alexander Fast d, Dmitry A. Fishman d, Valentine I. Vullev ORCID logoc, Maria Abrahamsson ORCID logoa, "CdS/ZnS core–shell nanocrystal photosensitizers for visible to UV upconversion," *Chem. Sci.*, no. 8, pp. 5488–5496, 2017.

[17] B. C. G. G. Blasse, *Luminescent Materials*. 1994.

[18] B. M. Walsh, "Judd-Ofelt theory: principles and practices brian m. walsh," *Int. Sch. At. Mol. Spectrosc.*, no. June, pp. 403–433, 2006.

[19] X. Li, F. Zhang, and D. Zhao, "Highly efficient lanthanide upconverting nanomaterials: Progresses and challenges," *Nano Today*, vol. 8, no. 6, pp. 643–676, 2013.

[20] B. D. Di Bartolo, J. Collins, and L. Silvestri, "Nano-structures for optics and photonics: Optical strategies for enhancing sensing, imaging, communication and energy conversion," *Nano-Structures Opt. Photonics Opt. Strateg. Enhancing Sensing, Imaging, Commun. Energy Convers.*, pp. 1–586, 2015.

[21] J. Collins, "Nano-Optics for Enhancing Light-Matter Interactions on a Molecular Scale," pp. 315–332, 2013.

[22] G. Blasse and B. C. Grabmaier, "How Does a Luminescent Material Absorb Its Excitation Energy?," *Lumin. Mater.*, no. Y 203, pp. 10–32, 2011.

[23] B. M. Van Der Ende, L. Aarts, and A. Meijerink, "Lanthanide ions as spectral converters for solar cells," *Phys. Chem. Chem. Phys.*, vol. 11, no. 47, pp. 11081–11095, 2009.

[24] J. Chen and J. X. Zhao, "Upconversion nanomaterials: Synthesis, mechanism, and applications in sensing," *Sensors*, vol. 12, no. 3, pp. 2414–2435, 2012.

[25] Shriver & Atkins, *Inorganic Chemistry*. .

[26] J. K. P.Atkins J. Paula, *Atkins Physical Chemistry, 11th edition, Oxford University Press*. .

[27] P. W. Atkins., *Physical chemistr, sixth edition, Oxford University Press*. 1998.

[28] J. d. P. P.Atkins, *Atkins Physical Chemistry, seventh edition, Oxford University Press*. .

[29] F. Auzel, "Upconversion and Anti-Stokes Processes with f and d Ions in Solids," *Chem. Rev.*, vol. 104, no. 1, pp. 139–174, 2004.

[30] S. Wen, J. Zhou, K. Zheng, A. Bednarkiewicz, X. Liu, and D. Jin, "Advances in highly doped upconversion nanoparticles," *Nat. Commun.*, vol. 9, no. 1, 2018.

[31] X. Wang, R. R. Valiev, T. Y. Ohulchanskyy, H. Ågren, C. Yang, and G. Chen, "Dye-sensitized lanthanide-doped upconversion nanoparticles," *Chem. Soc. Rev.*, vol. 46, no. 14, pp. 4150–4167, 2017.

[32] M. Haase and H. Schäfer, "Upconverting nanoparticles," *Angew. Chemie - Int. Ed.*, vol. 50, no. 26, pp. 5808–5829, 2011.

[33] and M. P. H. M. Pollnau, D. R. Gamelin, S. R. Lüthi, H. U. Güdel, "Power dependence of upconversion luminescence in lanthanide and transition-metal-ion systems," *Phys. Rev. B*, vol. 61, p. 3337, 2000.

[34] F. T. Rabouw, P. T. Prins, P. Villanueva-Delgado, M. Castelijns, R. G. Geitenbeek, and A. Meijerink, "Quenching Pathways in NaYF4:Er3+,Yb3+ Upconversion Nanocrystals," *ACS Nano*, vol. 12, no. 5, pp. 4812–4823, 2018.

[35] M. As. toyoJ. Fm. S Hinojosa, M.AMeneses-Nava, O Barbosa-García, L.ADíaz-Torres, "Energy back transfer, migration and energy transfer (Yb-to-Er and Er-to-Yb) processes in Yb,Er:YAG," *J. Lumin.*, vol. 102–103, pp. 694–698.

[36] Hai GuoNing DongMin YinWeiping ZhangLiren LouShangda Xia, "Visible Upconversion in Rare

Earth Ion-Doped Gd2O3 Nanocrystals," . *Phys. Chem. B*, vol. 108, no. 50, pp. 19205–19209, 2004.

[37] H. W. M. L.A. Risenberg, "Multiphonon Orbit-Lattice Relaxation of Excited States of Rare-Earth Ions in Crystals," *hopkins Univ. , Balt. marylad*, vol. 174, no. 2, 1968.

[38] G. Liu, "Advances in the theoretical understanding of photon upconversion in rare-earth activated nanophosphors," *Chem. Soc. Rev.*, vol. 44, no. 6, pp. 1635–1652, 2015.

[39] H. Dong, L. Sun, and C. Yan, "Chem Soc Rev Energy transfer in lanthanide upconversion," no. 2001, pp. 1608–1634, 2015.

[40] H. S. M. Haase, "Upconverting Nanoparticles," *Angew. Chemie - Int. Ed.*, vol. 50, pp. 5808–5829, 2011.

[41] P. K. S. iswapathik Pahari, Sandipan Chakraborty, Bidisha Sengupta, Sudip Chaudhuri, William Martin, Jasmine Taylor, Jordan Henley, Donald Davis, Pradip K. Biswas, Amit K. Sharma, "Biophysical Characterization of Genistein in Its Natural Carrier Human Hemoglobin Using Spectroscopic and Computational Approaches," 2013.

[42] X. Li, F. Zhang, and D. Zhao, "Lab on upconversion nanoparticles: Optical properties and applications engineering via designed nanostructure," *Chem. Soc. Rev.*, vol. 44, no. 6, pp. 1346–1378, 2015.

[43] M.J.Weber, "Probabilities for Radiative and Nonradiative Decay for Eu3+ in LaF3," *Phys. Rev.*, vol. 157, no. 2, 1967.

[44] X. Xie and X. Liu, "Photonics: Upconversion goes broadband," *Nat. Mater.*, vol. 11, no. 10, pp. 842–843, 2012.

[45] W. Zou, C. Visser, J. A. Maduro, M. S. Pshenichnikov, and J. C. Hummelen, "Broadband dye-sensitized upconversion of near-infrared light," *Nat. Photonics*, vol. 6, no. 8, pp. 560–564, 2012.

[46] T. Y. O. Xindong Wang, Rashid R. Valiev, "Dye-sensitized lanthanide-doped upconversion nanoparticles," *Chem. Soc. Rev.*, no. 14, 2017.

[47] T. Rinkel, J. Nordmann, A. N. Raj, and M. Haase, "Ostwald-ripening and particle size focussing of sub-10 nm NaYF4 upconversion nanocrystals," *Nanoscale*, vol. 6, no. 23, pp. 14523–14530, 2014.

[48] R. G. Geitenbeek, P. T. Prins, W. Albrecht, A. Van Blaaderen, B. M. Weckhuysen, and A. Meijerink, "NaYF4:Er3+,Yb3+/SiO2 Core/Shell Upconverting Nanocrystals for Luminescence Thermometry up to 900 K," *J. Phys. Chem. C*, vol. 121, no. 6, pp. 3503–3510, 2017.

[49] R. D. & X. L. Feng Wang, "Preparation of core-shell NaGdF4 nanoparticles doped with luminescent lanthanide ions to be used as upconversion-based probes," *Nat. Protoc.*, vol. 9, pp. 1634–1644, 2014.

[50] Z. Wang and A. Meijerink, "Dye-Sensitized Downconversion," *J. Phys. Chem. Lett.*, vol. 9, no. 7, pp. 1522–1526, 2018.